2014

Gas-Gas Separation Using a Hollow Fiber Membrane

Abdulmohsen Alsaiari
Lehigh University

Gas-Gas Separation

Using a Hollow Fiber Membrane

by

Abdulmohsen O. Alsaiari

A Thesis

Presented to the Graduate and Research Committee

of Lehigh University

in Candidacy for the Degree of

Master of Science

in

Mechanical Engineering

Lehigh University

May 2014

This thesis is accepted and approved in partial fulfillment of the requirement for the Master of Science in Mechanical Engineering.

_____

Date Approved

_____

Prof. Alparslan Oztekin

Advisor

_____

Dr. D. Gary Harlow, Chairperson

Mechanical Engineering and Mechanics

Table of Contents

List of Figures

Acknowledgements

First, I would like to thank God almighty for providing me with the physical and mental strength to complete this thesis and fulfill the requirements for my Masters Degree from a distinguished institution of Lehigh University. I thank him for Omar Alsaiari and Latifah Sultan; the wonderful parents he blessed me with who provided me with guidance and emotional support through my study. I thank him for the lovely wife Nouf Binthabit and the amazing son Salman who both were both a source of joy and support that, always, eased some of the stress accompanied my study

Also, the author wishes to express his appreciations to his advisor, Professor Alparslan Oztekin, for his encouragement and assistance in researching the topic of this thesis. He would also like to acknowledge colleague Nawaf Alkhamis for his help in working with ANSYS and related software. Such help was truly invaluable and made possible the swift completion of this thesis.

Finally, an extended thanks and appreciations to King Abdulaziz University for providing the financial support that was essential and provided me the chance to complete my Master of Science Degree at the institute of Lehigh University.

Nomenclature

C	Concentration [-]
J	Membrane Mass Flux [kg $s^{-1}m^{-2}$]
K	Permeability [m^2]
m	Mass [kg]
P	Pressure [Pa]
ΔP	Pressure difference [Pa]
p	Partial Pressure [Pa]
S	Mass Permeability [m^3(STP) m m^{-2} $s^{-1}Pa^{-1}$]
D	Mass Diffusion rate [kg m^{-1} s^{-1}]
RR	Rejection Rate [-]
h_m	Mass Transfer Coefficient [kg m^{-1} s^{-1}]
Sh	Sherwood Number [-]
A	Surface Area [m^2]
T	Porous Layer Thickness [m]
l	Membrane thickness [m]
R	Hollow Fiber Radius [m]
d	Hollow Fiber Diameter [m]
Z	Hollow Fiber Length [m]
H	Channel Height [m]
Re	Reynolds Number [-]

V	Velocity Victor [m s^{-1}]
u	Axial Velocity component [m s^{-1}]
v	Radial Velocity component [m s^{-1}]
U_{av}	Inlet Average velocity [m s^{-1}]
V_w	Membrane Suction Velocity [m s^{-1}]
z	z-Direction [-]
r	r-Direction [-]
μ	Viscosity [kg $m^{-1}s^{-1}$]
υ	Kinematic Viscosity [m^2 s^{-1}]
ρ	Density [kg m^{-3}]
α	Selectivity [-]
r*	Normalized Radius (r/R) [-]
z*	Membrane Normalized Length (z/Z) [-]
D*	Channel Normalized Permeability (K/H^2) [-]
Dp*	Porous Layer Normalized Permeability (K/T^2) [-]
u*	Normalized Axial Velocity (u/U_{av}) [-]
Vw*	Normalized wall Velocity (Vw/U_{av}) [-]

Subscript

a	Species: CO_2 or CH_4
b	Species: CO_2 or CH_4
a/b	Ratio of Properties of a to Properties of b
CO_2	Properties of CO_2

CH_4 Properties of CH_4

w Properties at Membrane Surface

Abstract

Computational fluid dynamics simulations are conducted for laminar steady asymmetric flows within a hollow fiber membrane unit. The goal is to study the effect of the porous layer of a hollow fiber membrane (HFM) on the flow regimes and thus on the separation process. The mixture of CH_4 and CO_2 is studied with the goal of separating CO_2 from CH_4. The hollow fiber membrane consists of a circular channel bounded by a supporting porous layer. Outer surface of the tubular pipe is bounded by a selective membrane. The Navier-Stokes equation, Darcy's law, and the species transport equations are solved for various values of permeability of the porous medium and Reynolds numbers. The mass flux of each species passing through the membrane is determined based on the local partial pressure, the concentration of each species, the permeability and the membrane selectivity. The porous layer influences the flow field in the open channel strongly. With increasing resistance the flow rate through the porous medium decreases. The flow rate through the open channel increases as the resistance of the porous layer is increased. The presence of the porous layer results in the reduction of mass flux of both CH_4 and CO_2 passing through the membrane. The Sherwood number is reduced at all Re as the resistance of the porous layer is increased. The increased resistance of the porous layer also causes an increase in the pressure drop in the hollow fiber membrane module. The present study proves that the porous layer should be included in modeling of hollow fiber membrane systems.

1. Introduction

The demand for natural gas is increasing as the world's power demand is increasing. It is a conservative estimate that 10% of today's world's energy consumption is sourced by the natural gas. However, row natural gas contains ethane, propane, butane, water vapor and acidic gases such as carbon dioxide and hydrogen sulphide. Acidic impurities in extracted natural gas can reach a concentration up to 4-50% of volume. Such levels of concentrations entail potential corrosion problems in the pipeline of transport [1]. Therefore, typical pipeline specifications usually mandate the concentration of carbon dioxide in natural gas to not exceed 2–5 volume percent [2]. This makes the removal of the acidic gases to be an essential process to preclude such problems.

The presence of water vapor with gases such as carbon dioxide and hydrogen sulphide creates an acidic milieu. Water vapor removal from the natural gas is conventionally attained by running the gas though a Glycol dehydration plant. Conventional method used to lower the concentration of acidic gases is amine gas treatment. However, membrane technology provides a practical alternative in which filtration and gas separation processes can be economical. Due to compactness and low investment cost, hollow fiber membranes (HMFs) are commonly used in gas separation and different filtration processes [3].

Hollow fiber membranes (HFM) represent a significant portion of the technology used in separation processes of CO_2 from natural gas. A single membrane consists of a circular cross-sectioned channel bounded by a supporting porous layer and both are

bounded by a selective membrane. A bundle of membranes is called a module; two practical flow configurations are absorption and desorption. In both configurations flows are either parallel or cross paths.

However, major disadvantages limit the use of HFMs in separation processes include membrane fouling and concentration polarization phenomena. This results in a reduction in permeated fluxes, membrane life, and efficiency. Such adverse effects make HFM applications to be undesirable for separation processes [4].

In this study, computational fluid dynamic simulations were conducted for an asymmetric hollow fiber membrane. Laminar flows of binary mixture consisting of CO_2 from CH_4 are considered. Several studies investigated and modeled similar problems using different approaches and models. Author views this work as an attempt to account for factors by which the separation process of a typical hollow fiber membrane may be affected. It proposes the solution of flow parameters using Darcy's equation in the porous support layer coupled with the solution of Navier-Stokes equation in the lumen side of the HFM. Proper membrane model are critical and applied as boundary conditions to obtain a solution of the mass transport across the membrane.

Flow characteristics in the lumen and in the porous medium can affect the separation process within a membrane composite. In the case of a separation process using a HFM, several studies employed Hagen- Poiseuille approximation to calculate pressure drop along the lumen side of a HFM. This approximation may result in a tangible calculation error for pressure drop along the lumen side because the walls of the membrane are assumed to be impermeable; commonly, the approximation was employed neglecting the effect of the porous support layer. In the present work, the model

computationally solved Navier-Stokes equation coupled with Darcy's equation s to calculate flow parameters of the membrane.

Kundu et al's in [5] and [6] model used a simplified approach in which a mass balance problem was considered over a differential length element of the HFM. Moreover, the model used Hagen- Poiseuille approximation and neglected the effect of the porous support layer. Thundyil and Koros [7] developed a model that used mass transport and mass balance equations but employed Hagen- Poiseuille approximation and neglected the effect of the porous support layer. C. Pan's [8] model considered a problem in which the flow is injected from the membrane into a channel. C. Pan had also used the Hagen- Poiseuille approximation to calculate the pressure drop.

Several studies used different approaches in which a mass diffusion problem was only considered. The effect of the mass transport on flow regimes at each side of the membrane was neglected. T. Sugiyama et al [9] computationally studied a transient vapor-air mass transport problem. The simulation only considered the transport problem at the membrane. H. Zhang et al [10], P. Keshavarz et al [11], A. Portugal et al [12], S. Shirazian et al [13], and B. Chen et al [14] all studied mass transport through the membrane by neglecting the effect of flow regimes on the transport. This was to simplify the solution of mass transfer by assuming fixed boundary conditions along the active separation layer of the membrane. However, several studies showed that flow parameters can be affected by the presence of parallel porous boundaries. Utilization of these studies can prove that it is important to investigate the effect of the flow and pressure field on the membrane performance. G. Beavers et al [15] experimentally studied coupled parallel flows in a channel and a bounding porous medium. Although their study did not include

any separation or filtration, it validated the slip boundary condition at the fluid-porous interface. S. Karode [16] developed an analytical solution for the pressure drop of a laminar flow in channels with porous walls. He assumed a constant flux permeated across the walls which he used as a boundary condition to calculate the pressure drop. Moreover, Karode developed the solution neglecting radial pressure gradient. The radial pressure gradient is a key factor influencing mass permeation across the walls. Number of studies used a CFD approach to solve coupled Navier-Stokes and Darcy equations. V. Nassehi [17] and R. Ghidossi et al [18] computationally solved coupled Navier-Stokes and Darcy flows for tubular channel bounded with porous walls. However, both studies considered only a filtration process through the walls without an active membrane as is considered for gas-gas separation. N.S. Hanspal et al [19] developed a computational model for the solution of flow equations in a two-dimensional fluid-porous coupled domain. However, the model also considered only a filtration process.

The effect of a porous support layer is expected mainly to affect the mass diffusion across the membrane by increasing flow resistance. B. Marcosa, et al [20] computationally solved Navier-Stokes and mass transport equations for a HFM used in an ultrafiltration system for protein concentration. The transient model accounted to flow resistances caused by polarization, blockage, and cake. However, the model did not incorporate the effect of a porous layer.

This work computationally investigates a tubular channel laminar flow that is bounded with porous walls. A selective membrane bounds both the channel and the porous walls. A solution for flow parameters in the lumen side (channel and porous walls) was obtained solving Navier-Stokes equations coupled with the Darcy's equation.

This solution was used as a boundary condition applied to a selective membrane at which fluxes of each component of a CO_2/CH_4 gas mixture are determined based on the local partial pressure and concentration, the permeability and the membrane selectivity. Mathematical model and assumptions are elaborately explained in the next section.

2. Mathematical Model

The schematic of the flow geometry is illustrated in Figure 1. It consists of a tubular channel bounded by porous walls and both are bounded by a dense membrane.

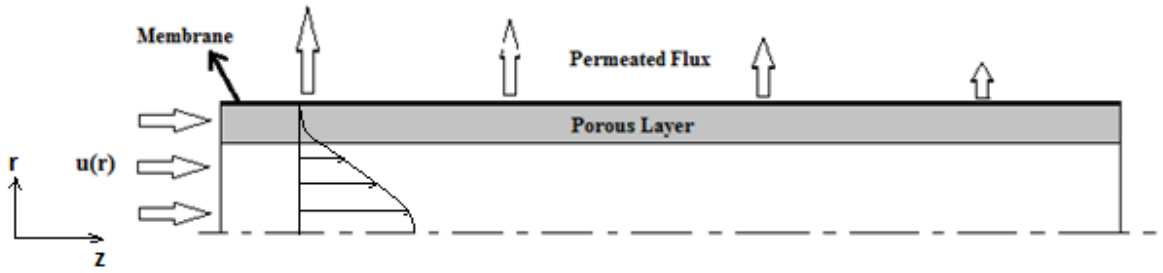

Figure 1: The schematic of the flow geometry.

Assumptions under which the model was developed are:

1. CH4 and CO2 are modeled as Newtonian fluids
2. Laminar flow
3. Isothermal and incompressible steady flow.
4. Density and diffusivity are independent of concentration.
5. Permeability is constant.
6. Total density of the binary mixture is constant
7. Axisymmetric flow – flow properties vary in r and z- directions.
8. Fully developed parabolic velocity profile at inlet.

9. Both radial and axial diffusion.

10. The porous layer is saturated.

11. The flow in the porous layer modeled by simple Darcy's Law

2.1 Governing equations

The equations governing fluid motion and the mass transport are:

Conservation of Mass

$$\nabla \cdot \mathrm{V} = 0 \tag{1}$$

Here V is the velocity vector and ∇ is the nabla operator. For the axisymmetric flow in a circular cross-sectioned pipe the equation (1) yields

$$\frac{1}{\mathrm{r}}\frac{\partial(\mathrm{rv})}{\partial \mathrm{r}} + \frac{\partial \mathrm{u}}{\partial \mathrm{z}} = 0 \tag{2}$$

where u and v are axial and the radial component of the velocity and r and z are the radial and axial coordinates.

Conservation of Momentum

The equation governing the mixture fluid motion in the open channel is Navier-Stokes equation in the form

$$\rho(\mathrm{V} \cdot \nabla)\mathrm{V} = -\nabla \mathrm{P} + \mu \nabla^2 \mathrm{V} \tag{3}$$

ρ is the total density of the mixture and is assumed to be constant. P is the static pressure, μ is the absolute or dynamic viscosity of the mixture and ∇^2 is the Laplace operator. The axial and radial components of the momentum equation are for the steady and axisymmetric laminar flow in the open pipe

$$\text{r-direction: } \rho\left(v\frac{\partial v}{\partial r}+u\frac{\partial v}{\partial z}\right)=-\frac{\partial P}{\partial r}+\mu\left[\frac{1}{r}\frac{\partial}{\partial r}\left(r\frac{\partial v}{\partial r}\right)-\frac{v}{r^2}+\frac{\partial^2 v}{\partial z^2}\right] \quad (4)$$

$$\text{z-direction: } \rho\left(v\frac{\partial u}{\partial r}+u\frac{\partial u}{\partial z}\right)=-\frac{\partial P}{\partial z}+\mu\left[\frac{1}{r}\frac{\partial}{\partial r}\left(r\frac{\partial u}{\partial r}\right)+\frac{\partial^2 u}{\partial z^2}\right] \quad (5)$$

Darcy's Law

Before introducing Darcy's law, it can be beneficial to familiarize with common terms used in the governing equations of a flow within porous mediums. A porous medium is a material consisting of a solid matrix with an interconnecting void space. The solid matrix can be assumed to be either rigid or undergoes small magnitude of deformation. Porosity and permeability are two terms commonly appear in governing equations of a flow within a porous medium. Porosity γ is defined as the ratio of a medium's void volume the total volume of that medium. If the medium is assumed to be isotropic, surface porosity also equals to volumetric porosity. Permeability K of a matter is defined as its ability to allow another substance, mostly a fluid, to pass through its pores. The SI unit of permeability is m^2. However, geologists prefer to measure permeability in units of a Darcy (1 Darcy = 0.987×10^{-12} m^2).

Henry Darcy (1856) was a French engineer with recognized contributions in the field of hydraulics. Through investigations and experimentations, Darcy developed an

expression that relates the velocity of a unidirectional flow, through a uniform porous medium, to the amount of applied pressure [21]. This relation is known as Darcy's law and it is of the form:

$$u = -\frac{K}{\mu}\frac{\partial P}{\partial x} \tag{6}$$

If the porous medium is assumed to be isentropic, permeability can be treated as a scalar and a general vector form of Darcy's law is written as:

$$\nabla P = -\frac{\mu}{K}V \tag{7}$$

Several deterministic and statistical models verified the validity of Darcy's law. However, number of studies argue that the linearity nature of Darcy's law holds verifiable results for a limited range of Reynolds numbers ($Re < O(10^2)$) [21]. Several empirical relations such as Brinkman's equation and Forchheimer's equation add a non linear term, extending Darcy's law, in order to account for inertial effects.

The simulation in the present study employs the Brinkman's equation in solving flow parameters, such as velocity and pressure drop, within a porous medium. The vector form of the Brinkman's equation is:

$$\nabla P = -\frac{1}{K}V + \frac{\tilde{\mu}}{\mu}\nabla^2 V \tag{8}$$

The first term in equation (8) is called the Darcy's term. However, the second term is viewed as an analogy to the Laplacian term that appears in the Navier-Stokes equation. In equation (8) $\tilde{\mu}$ is the effective viscosity and many factors are considered in determining

the value of $\frac{\tilde{\mu}}{\mu}$; Brinkman assigns a value of 1. Number of studies argue that the value of $\frac{\tilde{\mu}}{\mu}$ depends on the geometry and the porosity of the medium. Nield and Bejan in [21] discussed these studies concluding the applicability range of Brinkman's equation. In abstract, Brinkman's equation is preferable for porosity values > 0.6 and also for the study of flow behavior adjacent to the interface between the porous medium and the fluid. Moreover, Nield and Bejan concluded that Brinkman's equation reduces to Navier-Stokes equation as $K \to \infty$ and to Darcy's law as $K \to 0$.

In the current work of simulation, the porous layer has a porosity value of 0.4 and relatively low values of permeability. Considering these two factors make the application of Darcy's law a reasonable approximation for the calculation of flow parameters within the porous layer.

Inlet Velocity Profile

The velocity profile at the inlet is selected as the fully-developed Poiseuille profile for both in open pipe and the porous layer. Velocity and its gradient is assumed to be continuous at the interface between the open channel and the porous layer. The fully developed profile is derived from

$$\text{r-direction: } \rho\left(v\frac{\partial v}{\partial r} + u\frac{\partial v}{\partial z}\right) = -\frac{\partial P}{\partial r} + \mu\left[\frac{1}{r}\frac{\partial}{\partial r}\left(r\frac{\partial v}{\partial r}\right) - \frac{v}{r^2} + \frac{\partial^2 v}{\partial z^2}\right] \qquad (9)$$

Since the flow is assumed to be fully developed at the inlet ($\frac{\partial}{\partial z} = 0$), equation (9) reduces to:

$$\rho\left(v\frac{\partial v}{\partial r}\right) = -\frac{\partial P}{\partial r} + \mu\left[\frac{1}{r}\frac{\partial}{\partial r}\left(r\frac{\partial v}{\partial r}\right) - \frac{v}{r^2}\right] \quad (10)$$

From the continuity equation,

$$\frac{\partial(rv)}{\partial r} = 0 \rightarrow rv = C \quad (11)$$

Since v = 0 at r = R, thus v = 0 has to be zero everywhere for the fully-developed flow. Therefore, equation (10) yields $\frac{\partial P}{\partial r} = 0$; implying that P = P(z).

Therefore, the z-direction Navier-Stokes equation reduces to:

$$\frac{d}{dr}\left(r\frac{du}{dr}\right) = \frac{r}{\mu}\frac{dP}{dz} \quad (12)$$

Integrating equation (12) twice and applying the boundary conditions of u = 0 at r = R and $\frac{du}{dr} = 0$ at r = 0, the well-known Poiseuille velocity profile is obtained as

$$u(r) = -\frac{R^2}{4\mu}\left(\frac{dP}{dz}\right)\left(1 - \frac{r^2}{R^2}\right) \quad (13)$$

Equation (13) represents a fully developed velocity profile at the inlet of the hollow fiber membrane. However, expressing u(r) in terms of the flow's average inlet velocity U_{av} can be a better representation. The average inlet velocity U_{av} is expressed as:

$$U_{av} = \frac{2}{R^2}\int_0^R u(r) r\, dr \quad (14)$$

Substituting for u(r) from equation (13) into equation (14) as:

$$U_{av} = -\frac{2}{R^2}\int_0^R \left[\frac{R^2}{4\mu}\left(\frac{dP}{dz}\right)\left(1 - \frac{r^2}{R^2}\right)\right] r\, dr \quad (15)$$

Integrating equation (15) yields:

$$U_{av} = -\frac{R^2}{8\mu}\left(\frac{dP}{dz}\right) \tag{16}$$

Incorporating equation (16) into (13), it yields:

$$u(r) = 2U_{av}\left(1 - \frac{r^2}{R^2}\right) \tag{17}$$

Equation (17) is a practical expression of the inlet velocity profile. This is because U_{av} also can be expressed in terms of the fiber's diameter, flow's kinematic viscosity, and Reynolds number as $U_{av} = \frac{Re \cdot \upsilon}{d}$.

Mass Diffusion and Membrane Model

The equation governing the mass transport of the species "a" is of the form

$$D\nabla^2 C_a = V \cdot \nabla C_a \tag{18}$$

where D is the diffusion coefficient and C_a is the concentration of component "*a*" in a binary gas mixture of CH_4 and CO_2. For the axisymmetric mass transport, equation (18) cylindrical is of the form

$$D\left[\frac{1}{r}\frac{\partial}{\partial r}\left(r\frac{\partial C_a}{\partial r}\right) + \frac{\partial^2 C_a}{\partial z^2}\right] = u\frac{\partial C_a}{\partial z} + \frac{v}{r}\frac{\partial}{\partial r}(r\,C_a) \tag{19}$$

The flux of species "a" across a membrane is determined by:

$$J_a = \frac{S_a}{l}\left(p_a^{(1)} - p_a^{(2)}\right) \tag{20}$$

Where J_a is the mass flux of the species "a" per unit area, l is the membrane thickness S_a is the mass permeability of the species "a", $\Delta p_a = \left(p_a^{(1)} - p_a^{(2)}\right)$ is the partial pressure difference across the membrane for the species "a". Species "a" can be either CO_2 or CH_4.

The surface mass suction rate of the membrane per unit area is determined as:

$$m_w = J_{CO_2} + J_{CH_4} = \frac{S_{CO_2}}{l}\Delta p_{CO_2} + \frac{S_{CH_4}}{l}\Delta p_{CH_4} \quad (21)$$

Here m_w is the total mass suction rate at the membrane surface and it can be written as:

$$m_w = \frac{S_{CO_2}}{l}\left[\alpha\Delta p_{tot} + (1-\alpha)\Delta p_{CO_2}\right] \quad (22)$$

With membrane selectivity α defined as

$$\alpha = S_{CH_4}/S_{CO_2} \quad (23)$$

and the total partial pressure is determine as:

$$\Delta p_{tot} = \Delta p_{CH_4} + \Delta p_{CO_2} \quad (24)$$

The concentration of species "a" at the membrane's wall is related to the concentration gradient at the wall by:

$$D\frac{\partial C_a}{\partial r} = (RR)V_w C_a \quad (25)$$

where the suction velocity at the surface of the membrane is determined by

$$V_w = \frac{m_{w,CO_2}}{\rho_{CO_2}} + \frac{m_{w,CH_4}}{\rho_{CH_4}} \quad (26)$$

Here RR is the rejection rate of species "a" and it is usually assumed to be constant in the membrane modeling for liquid applications such as desalination. This is because the concentration of solute is very small compared to the solvent. However, the case is different for membranes used in the gas-gas separation applications where the rejection rate should rather be a function of the partial pressure of both species along the surface of membrane as:

$$\mathrm{RR} = \frac{J_b - J_a}{J_b + J_a} \tag{27}$$

Using equations (20) to (26) into the rejection rate can be written as:

$$\mathrm{RR} = \frac{\Delta p_{CO_2} - \alpha \Delta p_{CH_4}}{\alpha \Delta p_{tot} + (1-\alpha)\Delta p_{CO_2}} \tag{28}$$

Substituting equations (22) and (27) into (25) it yields a boundary condition for the concentration for species "a" as:

$$D\frac{\partial C_a}{\partial r} = \frac{S_{CO2}}{l}(\Delta p_{CO_2} - \alpha \Delta p_{CH_4})C_a \tag{29}$$

The mass transfer coefficient and the corresponding local Sherwood number are calculated as:

$$h_m(z) = \frac{D\frac{\partial C_a}{\partial r}(z)}{(C_m(z) - C_w(z))} \tag{30}$$

$$\mathrm{Sh}(z) = \frac{h_m(z)d}{D} \tag{31}$$

where h_m is the local mass transfer coefficient, C_m is local the bulk concentration of the species “a”, C_w is the local wall concentration and Sh is the local Sherwood number.

3. Numerical Model

3.1 Computational Fluid Dynamics

Computational fluid dynamics (CFD) is a commonly used tool to obtain numerically approximated solutions to heat transfer and fluid dynamics problems. Before (CFD), obtaining solutions to these problems used to be a lengthy and tedious process; these problems were solved by hand with the help of tables. The earliest use of (CFD) was in the solution of one-dimensional equations for military problems in the first half of the twentieth century. Due to improvements in computing capabilities, two- and three-dimensional problems were solved by the end of the 1960s and the 1980s [22]. Today, many students and professionals use a variety of CFD packages on a daily basis.

3.2 Geometry and Mesh

The use of CFD involves a sequence of steps. The first step is the creation of the simulation geometry. This is usually done using Computer-Aided Design (CAD) modeling software. After the creation of the geometry, a mesh is then created for the geometry. The user is required to determine an appropriate number of elements to be used in a mesh. The resolution of a mesh is usually defined by the number of elements (or nodes) the simulation geometry was divided into. Having higher resolutions means having more elements. This generally enhances a solution's accuracy but also corresponds to higher computational times. The user is ought to find a balance between solution's accuracy and mesh resolution. This is in order to produce results with a reasonable accuracy and a practical amount of time. Moreover, the user should study the

convergence of the solution obtained. This is done by running the simulation model for different values of mesh resolution. Starting with lower values of resolutions, the solution should be observed for noticeable changes. If the obtained solution is not changed noticeably as the mesh resolution increases, then the solution is said to be independent of the mesh resolution. Figure 2 displays the proof of mesh independence of the present simulations. The stream-wise and the span-wise velocity profiles predicted using different mesh sizes are plotted at z/d = 60 for Re = 400. There is no discernible difference in the velocity profiles for mesh sizes varying from 200,000 nodes to 800,000 nodes. The results presented in the present study are obtained using 500,000 nodes.

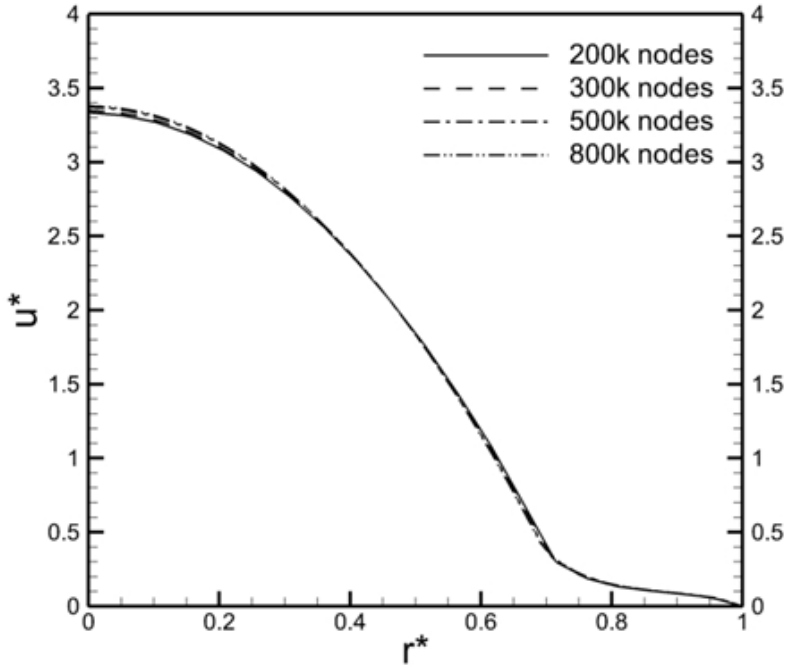

a) The normalized stream-wise velocity

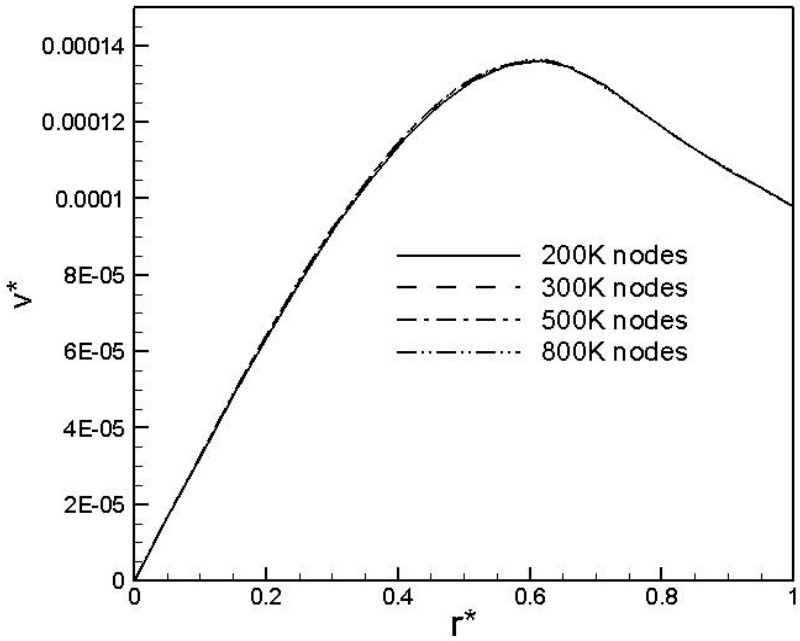

b) The normalized span-wise velocity

Figure 2: Velocity profiles at z/d = 60 for different mesh sizes.

In the present study, the computational domain has a diameter to length ratio of 120. The diameter of the hollow fiber membrane is 1mm and the length is 120mm. The total objected surface area of which a mesh was created for is 60mm^2. This area is divided into 500,000 rectangular elements; an optimum mesh resolution is found to be 8,333 $\frac{\text{elments}}{\text{mm}^2}$, as seen in Figure 3. Uniform mesh through the open pipe and the porous layer are used.

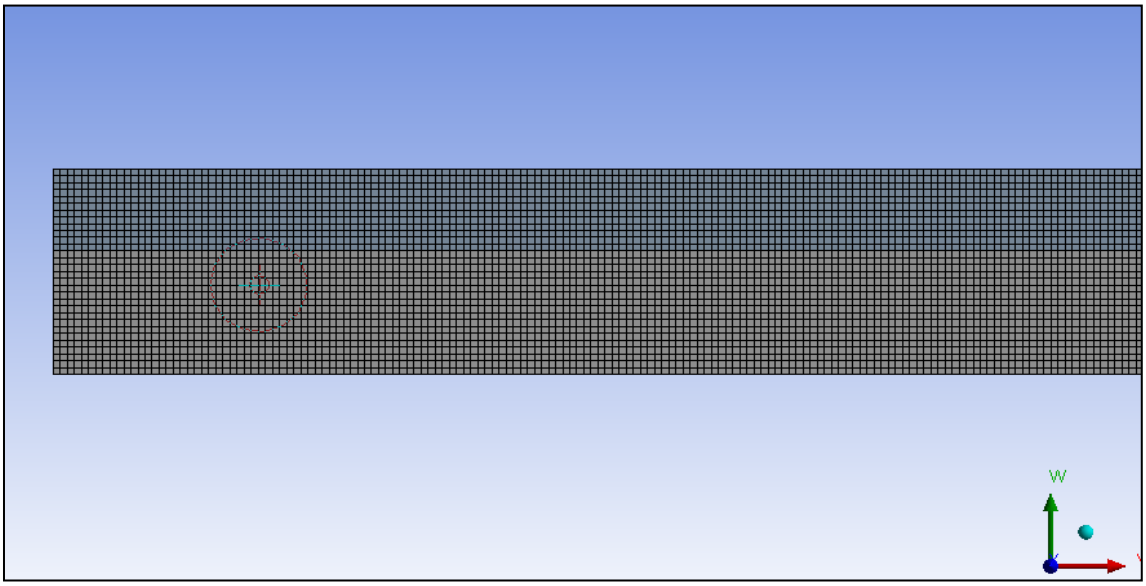

Figure 3: Mesh created with ANSYS.

3.3 Numerical model and the boundary conditions

To accurately simulate a problem, an optimum numerical model should to be selected. This is generally done by the determination whether the problem considered is a transient or a steady-state and whether the flow is laminar or turbulent. In the present study a steady laminar flow in a circular cross-sectioned pipe surrounded by a porous

layer is examined. The flow system is bounded by the membrane. The boundary conditions imposed on the velocity field along the membrane is modeled by treating the membrane as a functional surface. The mass flux through the membrane depends on the local flow conditions and the concentration. After that, boundary conditions are applied to the problem; special attention should be given to the condition at the inlet and outlet. The boundary conditions imposed on the velocity and the concentration fields are listed in Table 1.

Parameter	**Range of values**
Permeability (m^2),	[10^{-7}, 10^{-8}, and 10^{-9}]
Inlet Reynolds number	[30-400]
Suction Pressure at the membrane surface (bar)	[-2.5]
Diameter and Length (mm)	[1 and 120], receptively
Flow Exist Pressure (bar)	[0]
CH4 Inlet Concentration (Volume %)	[70]
Membrane Selectivity	[0.0086]

Table 1: Boundary conditions imposed on the velocity and concentration

3.4 Solution procedure and the post-processing

Several softwares are available to conduct powerful computational fluid dynamics simulations: FLUENT, CFX, and OpenFOAM. Several inputs, such as the number of iterations, should be specified to perform the calculation of a solution. Values of properties of interest such as velocities and maximum cell residuals should be monitored

during iterations. A convergence is accomplished when residuals in flow parameters approach zero and properties of interest approach to expected values.

Once the solution is obtained, post-processing takes place. Results of the simulation can be represented in several ways; velocity and pressure contours, vector plots, performance parameters, etc. It is essential to make sure that the results displayed are reasonable and validated by comparing them with known analytical or experimental solutions obtained under similar conditions; otherwise, the solution's validity may fail.

4. Results and Discussion

Membrane and flow model used by the present study is validated by conducting two tests. Developing flow in a channel bounded by the membrane is simulated at Re = 150. The mixture of CH4 and CO2 is considered for the test. The porous layer is not included in the simulation. Away from the inlet, nearly fully developed conditions are attained. Sherwood number approaches to a nearly constant value. The Sherwood number predicted by this test agrees well with that obtained for the fully-developed laminar flow [23], as illustrated in Figure 4.

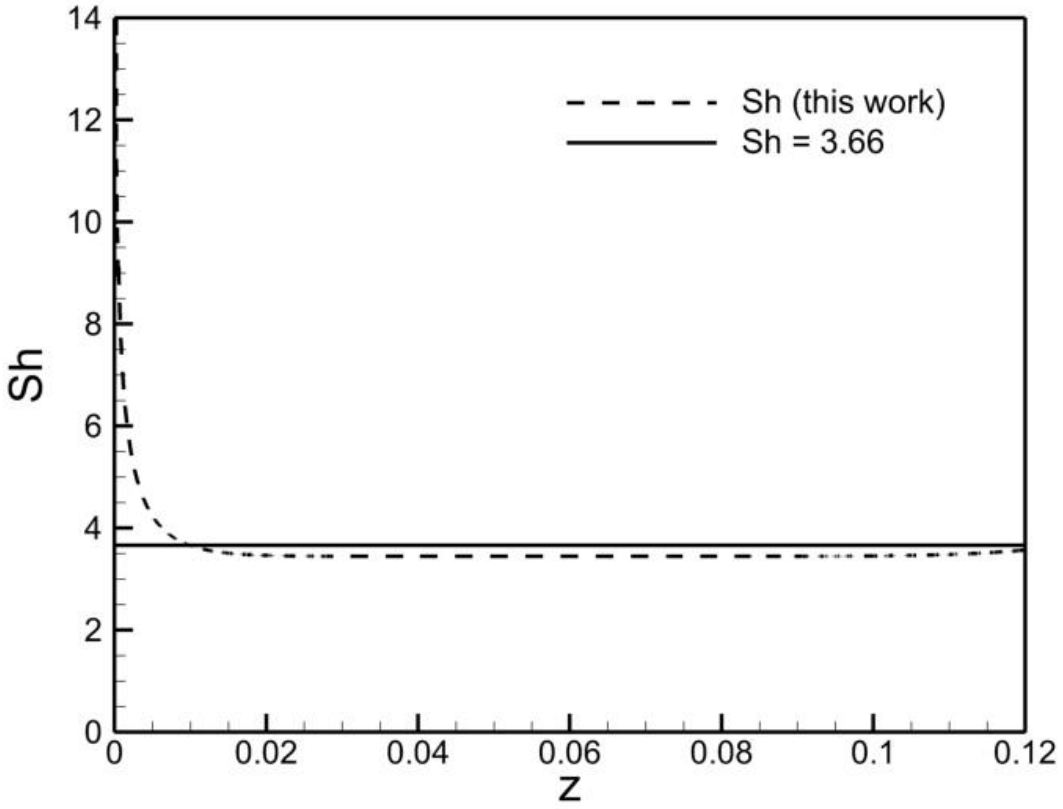

Figure 4: The local Sherwood number vs z/d at Re=150. Dashed line denotes the Sh for the developing flow predicted by the present study and dashed lines denote Sh for the fully-developed flow in a pipe for the constant flux at the surface.

In order to validate modeling flow in a channel surrounded by the porous layer another test is conducted by simulating laminar flow without the presence of the membrane. The velocity profiles in an open channel surrounded by the porous medium is calculated away from the inlet and compared against the results reported by E. Ucar et al [24]. Figure 4 shows fully-developed velocity profile obtained with CFX and a reasonable agreement is observed. Figure 4 depicts the velocity profile near the outlet for various values D* predicted by the present study. Here D* is dimensionless permeability of the porous medium and is defined by K/H^2 where K is the permeability and H is the height of the channel considered. These velocity profiles are very similar to those exact solutions of fully developed flows at the same condition obtained by the E. Ucar.

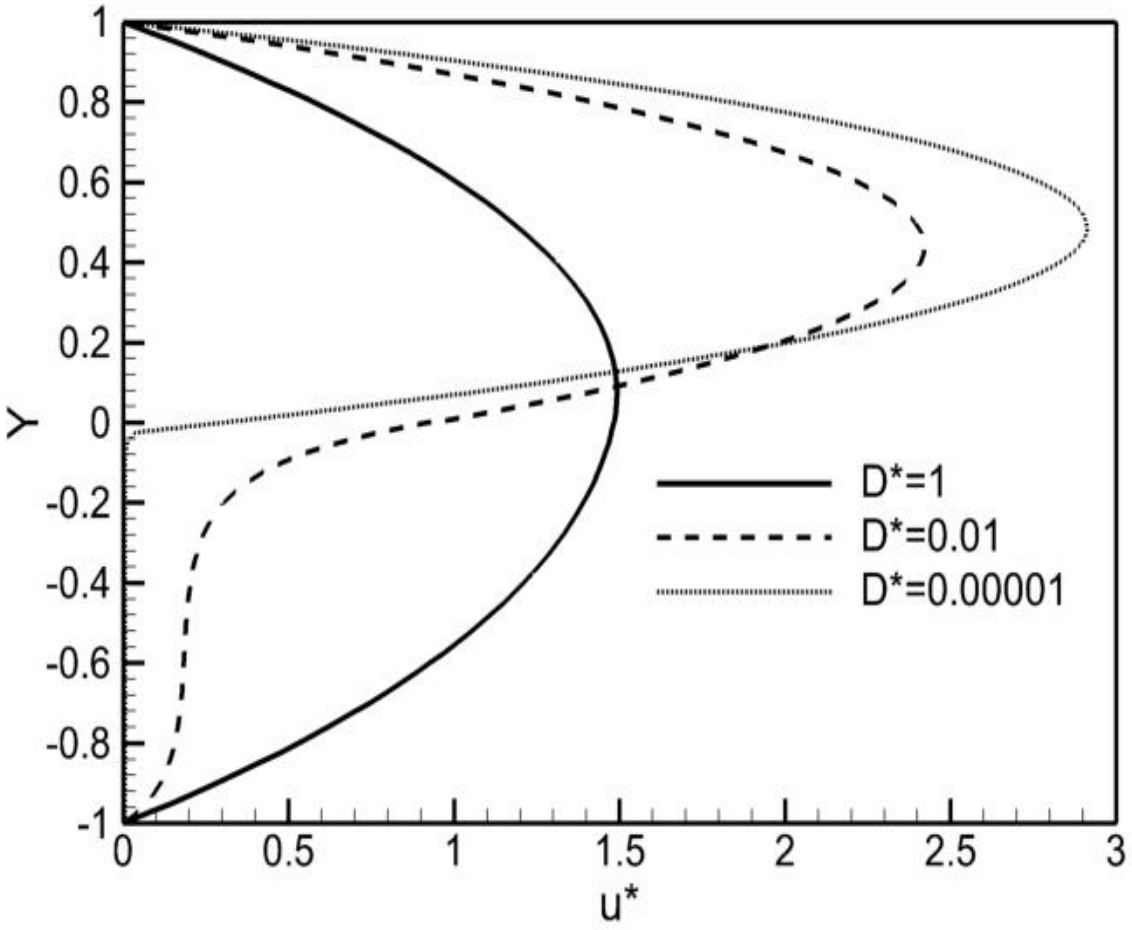

Figure 5: Stream-wise component of the velocity profile predicted for various values of D*.

Figures 6 to 8 illustrate the normalized streamwise component of velocity profiles at z/d = 60 for different values of dimensionless permeability of the porous layer, $Dp^* = \frac{K}{T^2}$. K is the permeability and T is the thickness of the porous wall. The thickness of the porous layer is fixed as 0.165mm and the permeability is varied to investigate the effect of Dp* on the flow structure in the open channel and the porous layer when the channel outer boundary is bounded by the membrane. The inlet velocity profile is selected to be a parabolic in both the open channel and the porous layer with a continuous

fluid speed and the continuous derivative. For low permeability (Dp*=0.037), the centerline fluid speed is increased significantly. It is noted that the centerline fluid speed is 70% of the maximum velocity obtained when there is no porous medium. It is also noted that the fluid speed inside the porous layer drops significantly as the porous layer becomes thicker, as depicted in the Figures for Dp* = 0.037. As the thickness of the porous layer increases or the permeability decreases the resistance against flow increases which results in drops in fluid speed and increase in pressure drop. Such flow characteristics is key factor in determining the membrane performance as presented below.

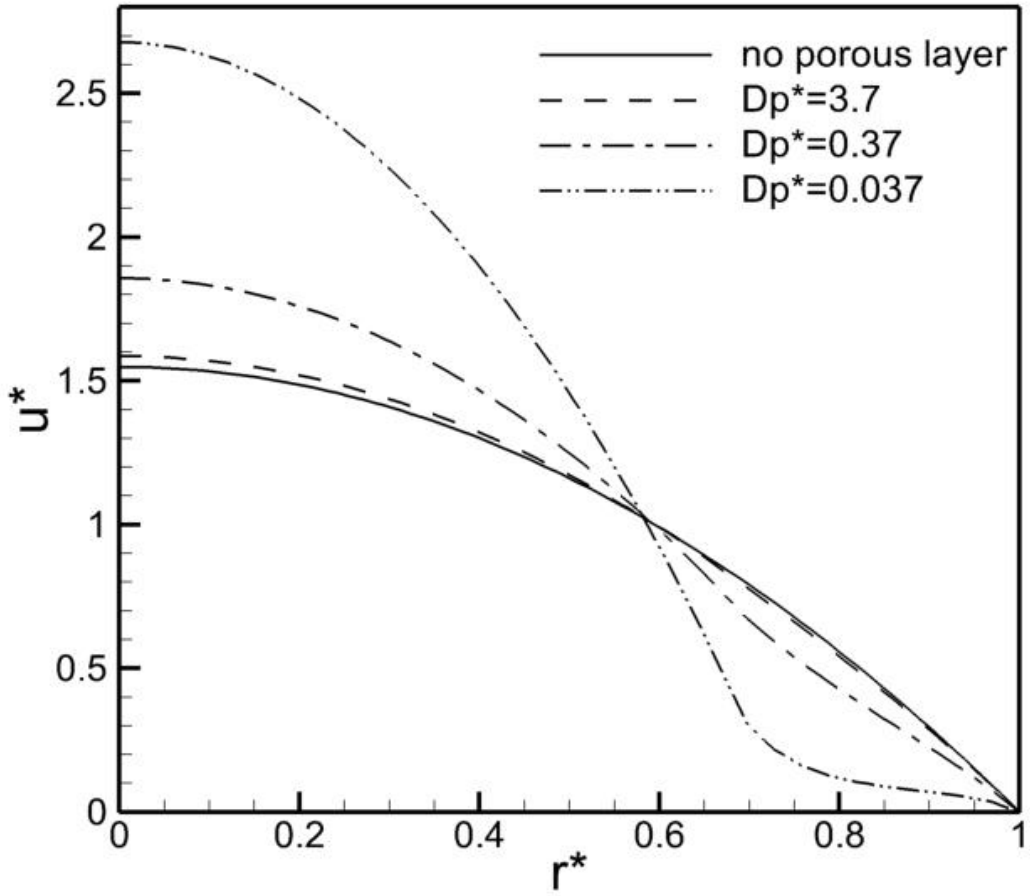

Figure 6: Normalized axial velocity profiles at z/d = 60 for different values of Dp* at Re =30.

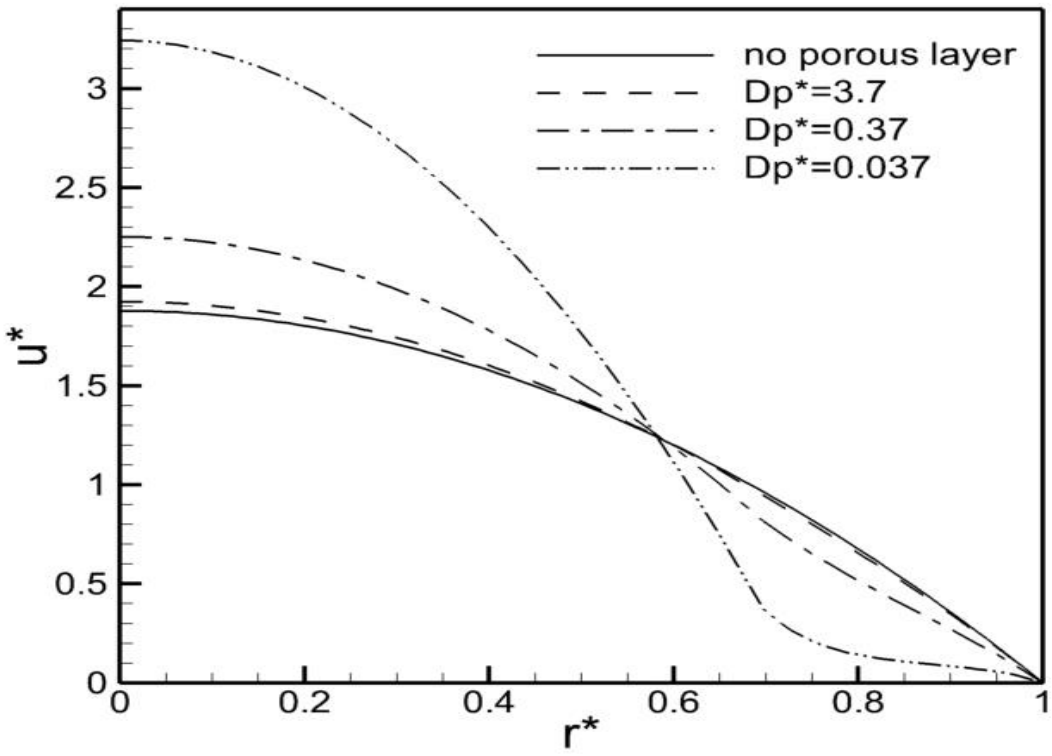

Figure 7: Normalized axial velocity profiles at z/d=60 for different values of Dp* at Re =150

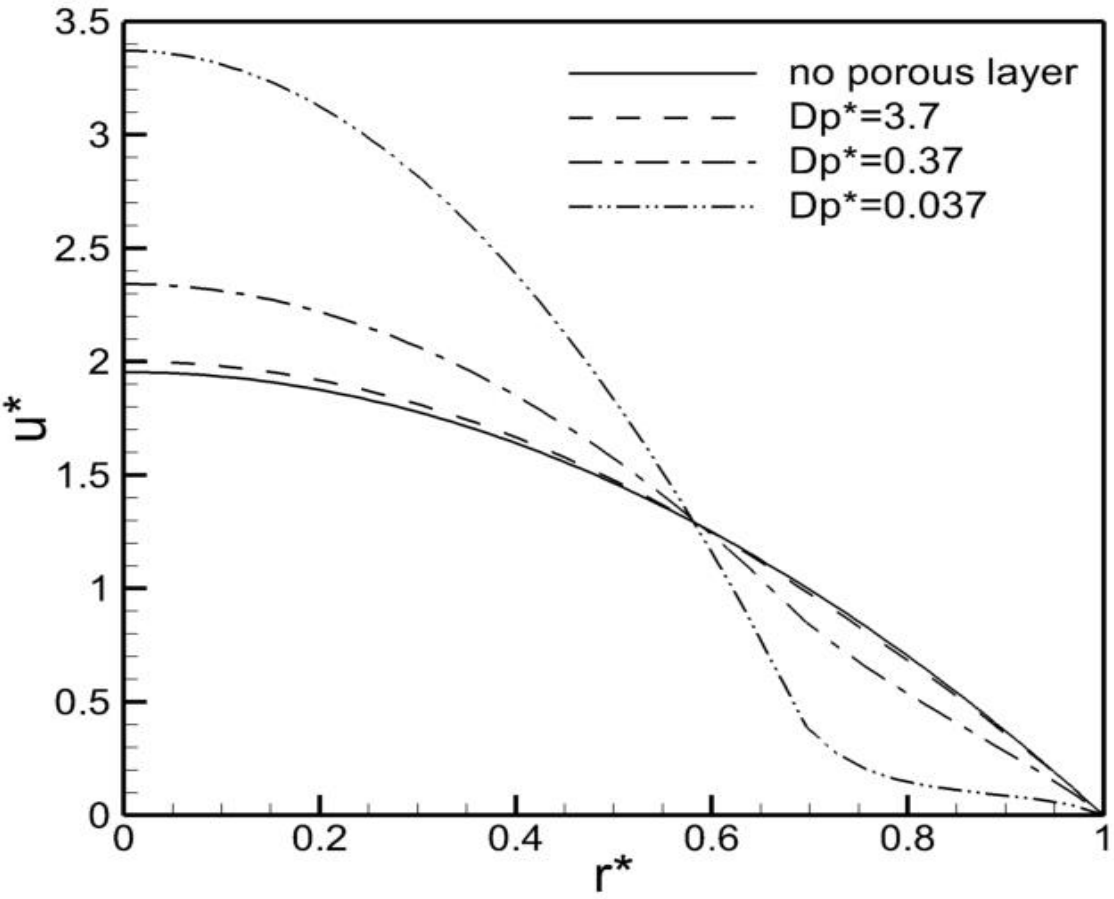

Figure 8: Normalized axial velocity profiles at z/d = 60 for different permeabilites and Re = 400

Figures 9 to 11 depict the effect of the suction along the membrane surface on the streamwise velocity calculated at different locations for Dp* =0.37. It has been shown here that the mass transport through the membrane has strong influence on flow regimes; the effect is manifested as a decrease in the streamwise velocity as z increases. Moreover, this decrease is more pronounce at low Re number flow, as seen in Figure 9. This is due to the fact that residence time of the mixture of CH_4 and CO_2 in the

computation domain icreases as Re is decreased. At Re = 400 there is a little change in the streamwise velocity profiles at various z locations, as seen in Figure 11.

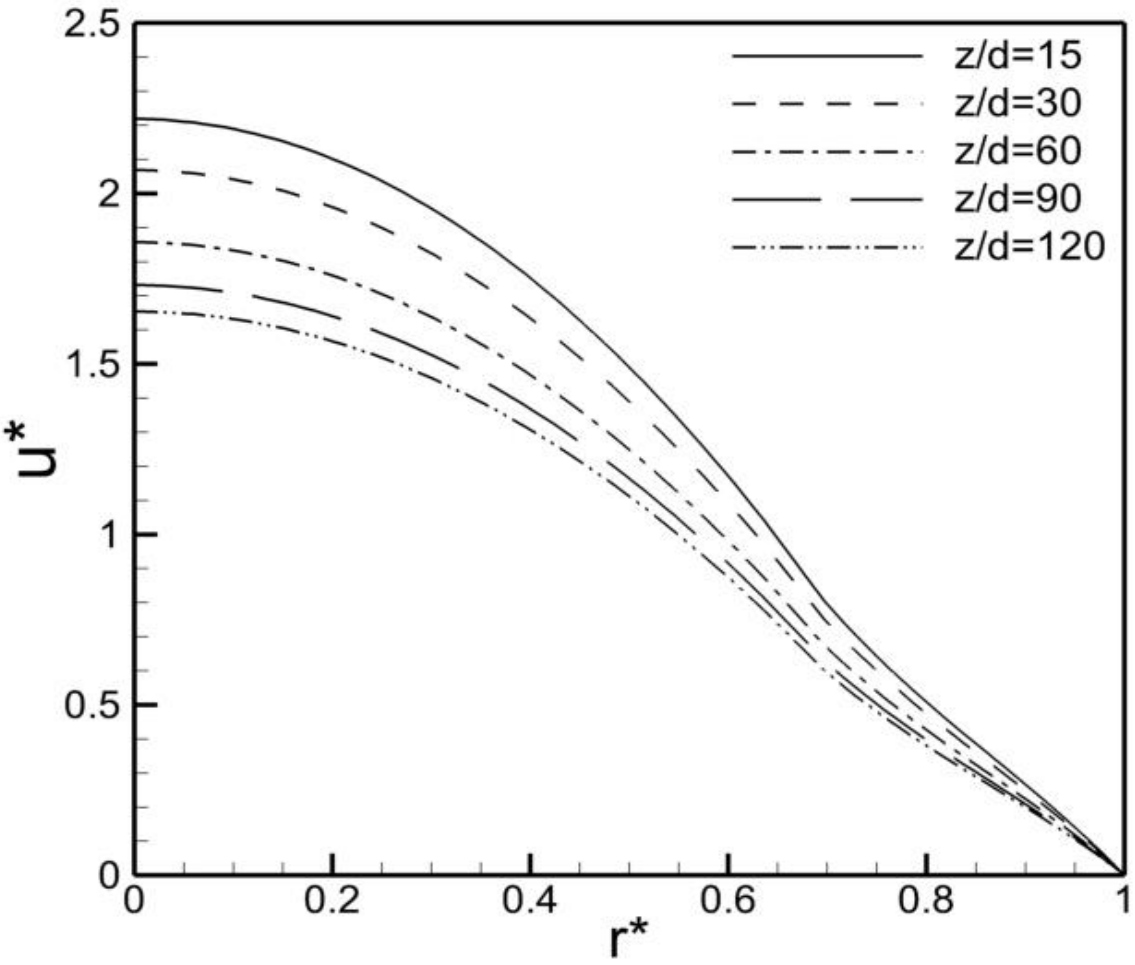

Figure 9: Normalized axial velocity profiles at z/d=15, 30, 60, 90, and 120 for Dp* =0.37 and Re =30

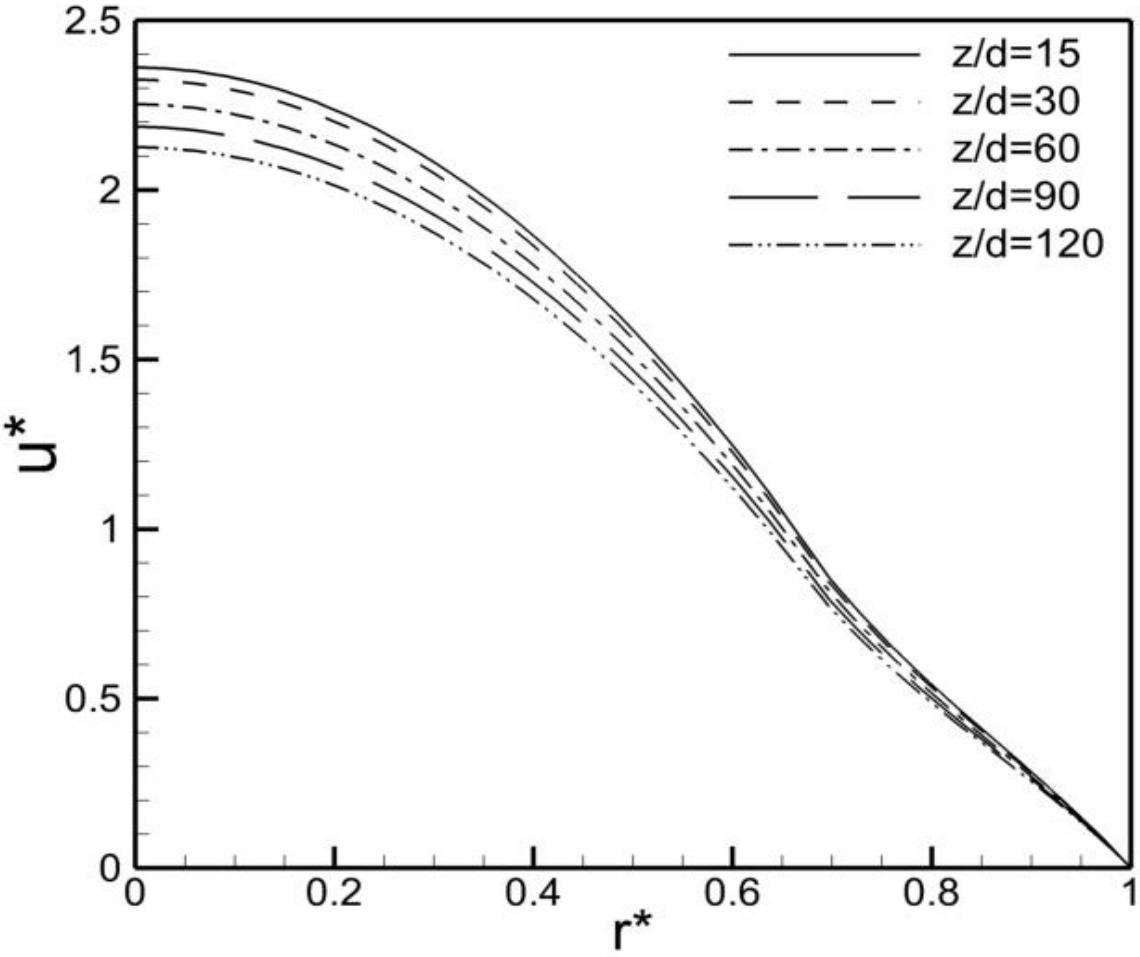

Figure 10: Normalized axial velocity profiles at z/d = 15, 30, 60, 90, and 120 for Dp* = 0.37 and Re =150.

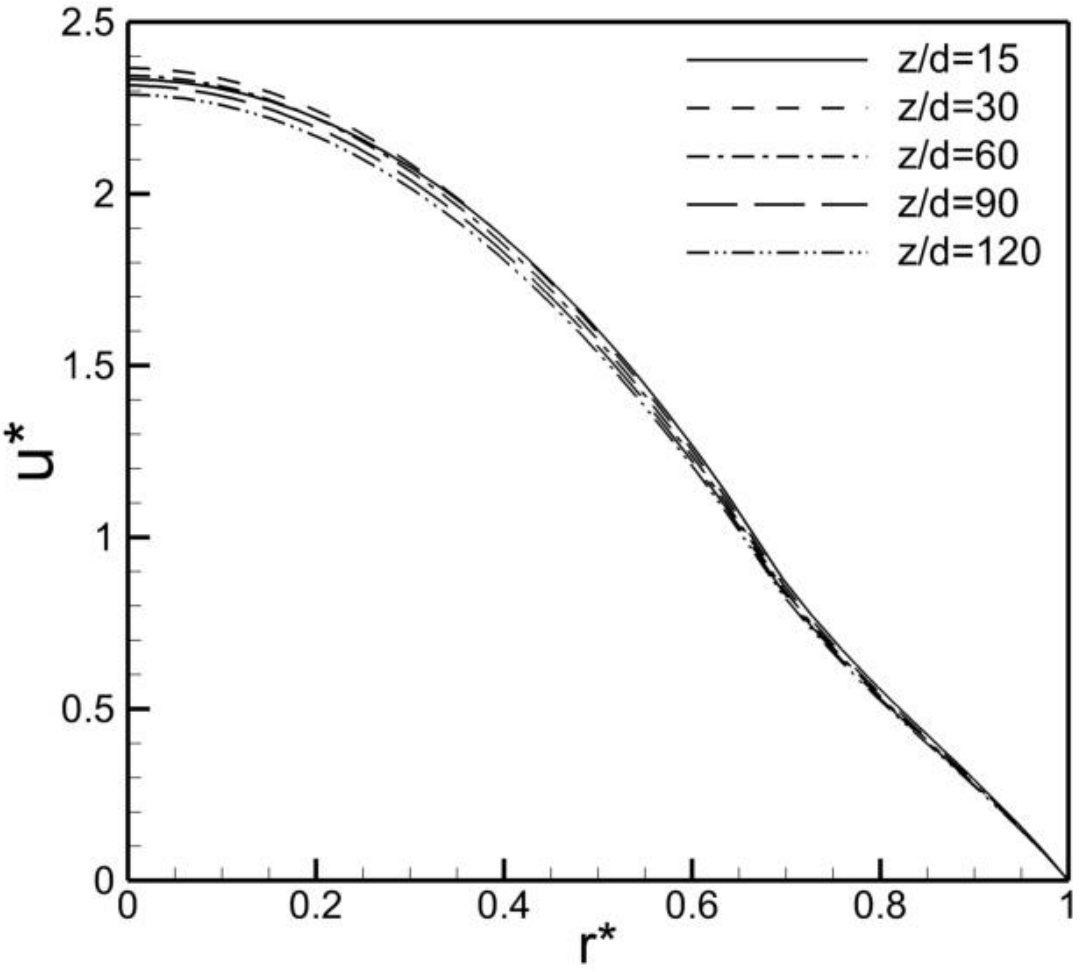

Figure 11: Normalized axial velocity profiles at z/d = 15, 30, 60, 90, and 120 for Dp* = 0.37 and Re =400.

Figures 12 to 14 illustrate CH_4 concentration profiles calculated at z/d = 60 for various values of Dp* including the case when there is no supporting porous medium for the membrane. Concentration of CH_4 is always highest at the membrane wall and the lowest at the center for all cases, as shown in Figures 12-14. Concentration of CH_4 is much lower at higher flow rates. This is due to the fact that residence time of the mixture of CH_4 and CO_2 in the computation domain selected here decreases as Re is increased.

The effect of Re is reversed as the permeability of the porous layer is varied. At lower Re flow, the mixture is CH_4 rich when there is no porous layer, as shown in Figure 12. As the porous layer becomes thicker or permeability becomes lower the level of CH_4, especially near the center of the channel, becomes lower. However, for higher Re flows mixture becomes CH_4 rich in the porous layer and the surface of the membrane, see Figures 13 and 14. Obviously, the level of CO_2 passage through the membrane increases as the flow speed in the open channel becomes higher. This clearly indicates that the effect porous support layer is profound on the performance of the membrane. Accurate flow modeling in the porous layer is necessary to determine how membrane in gas-gas separation performs.

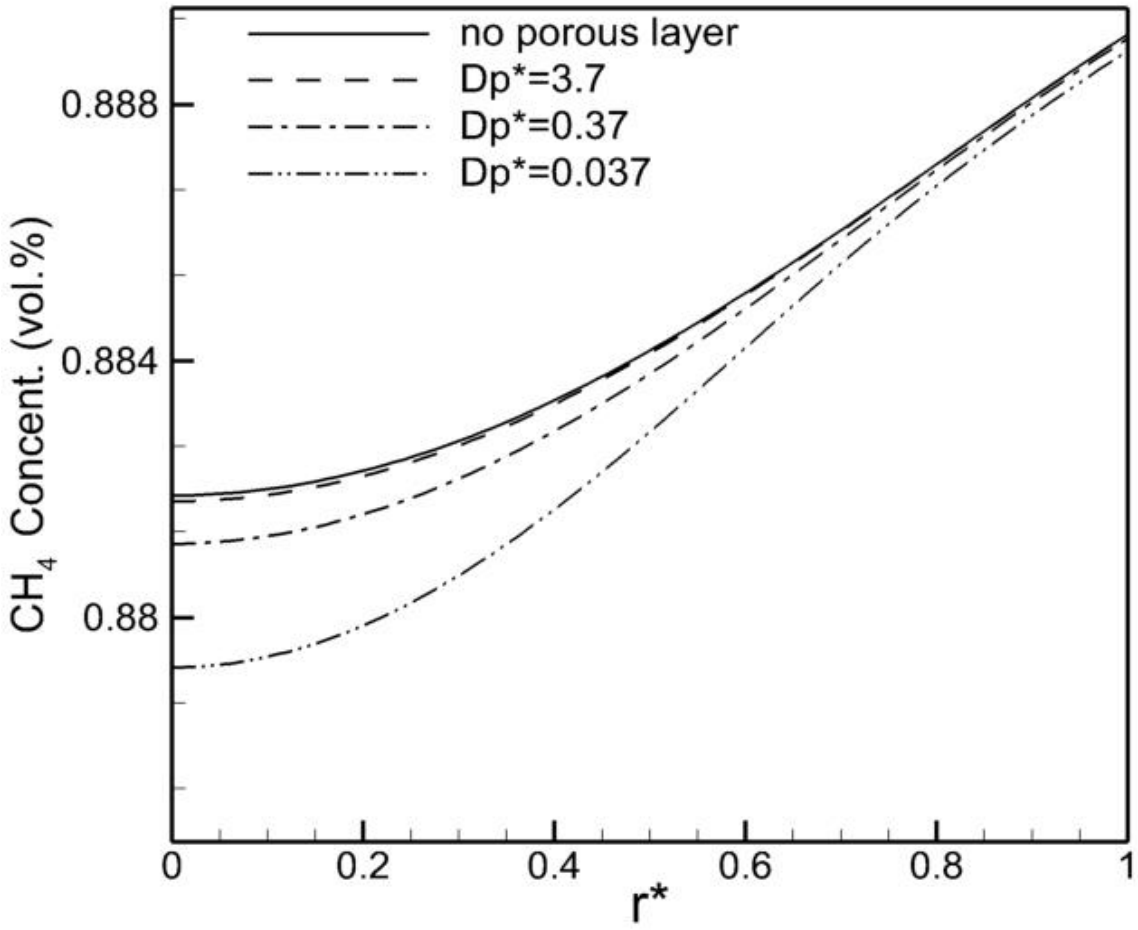

Figure 12: Concentration profiles at z/d=60 for different values of Dp* at Re =30.

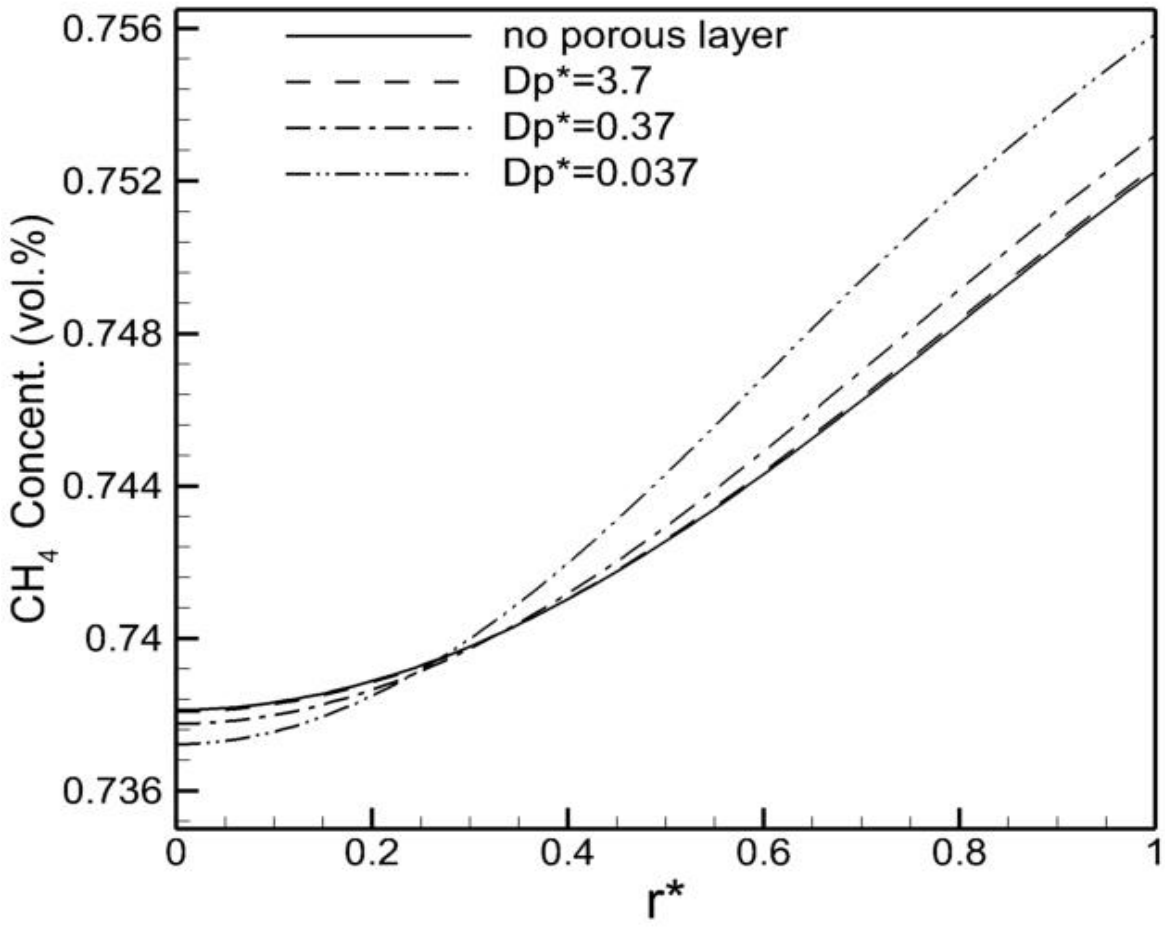

Figure 13: Concentration profiles at z/d = 60 for different values of Dp* at Re =150.

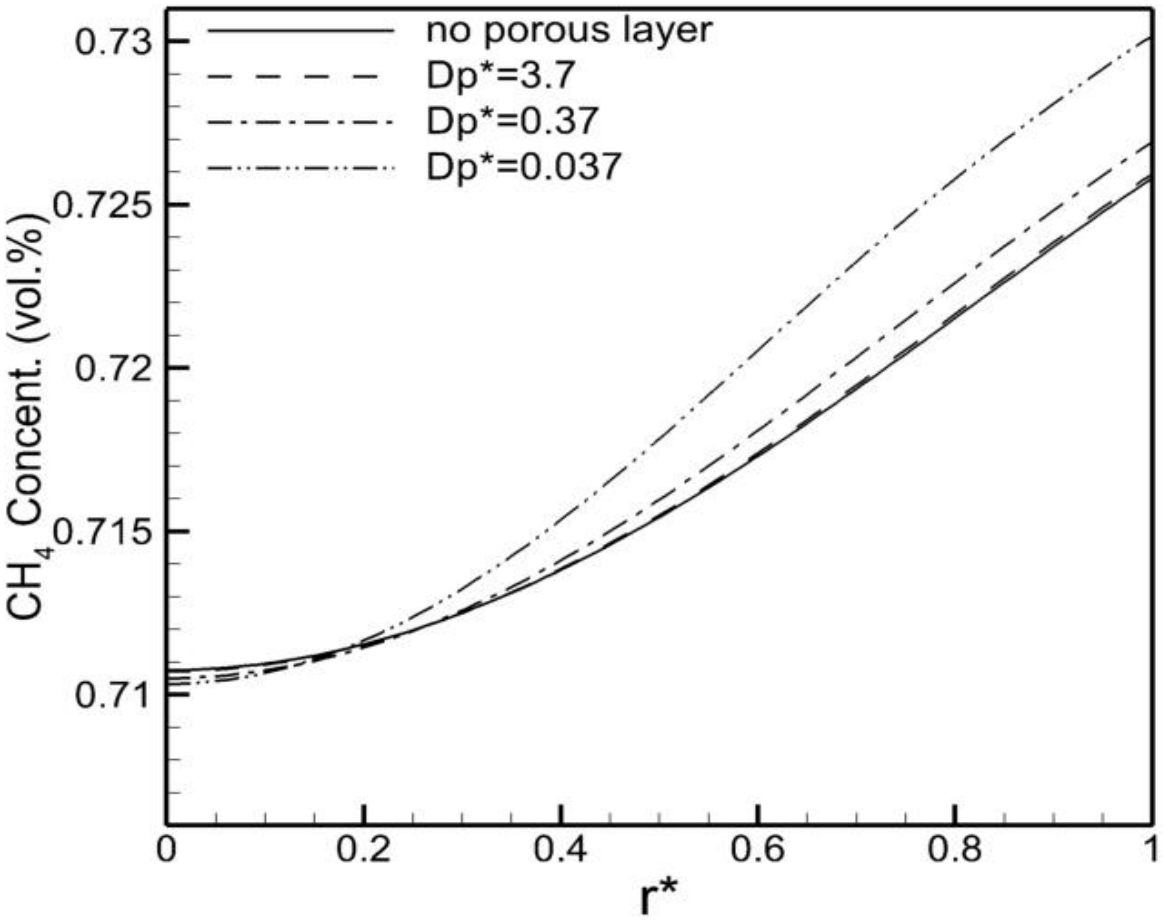

Figure 14: Concentration profiles at z/d = 60 for different values of Dp* at Re =400.

Figures 15 to 17 depict the suction rate for different values of Dp* at various Re. It is noted that the suction rate decreases as the Dp* becomes lower. This effect is more pronounced at high Re and lower Dp*. Moreover, the pressure drop is predicted to increase as Dp* decreases.

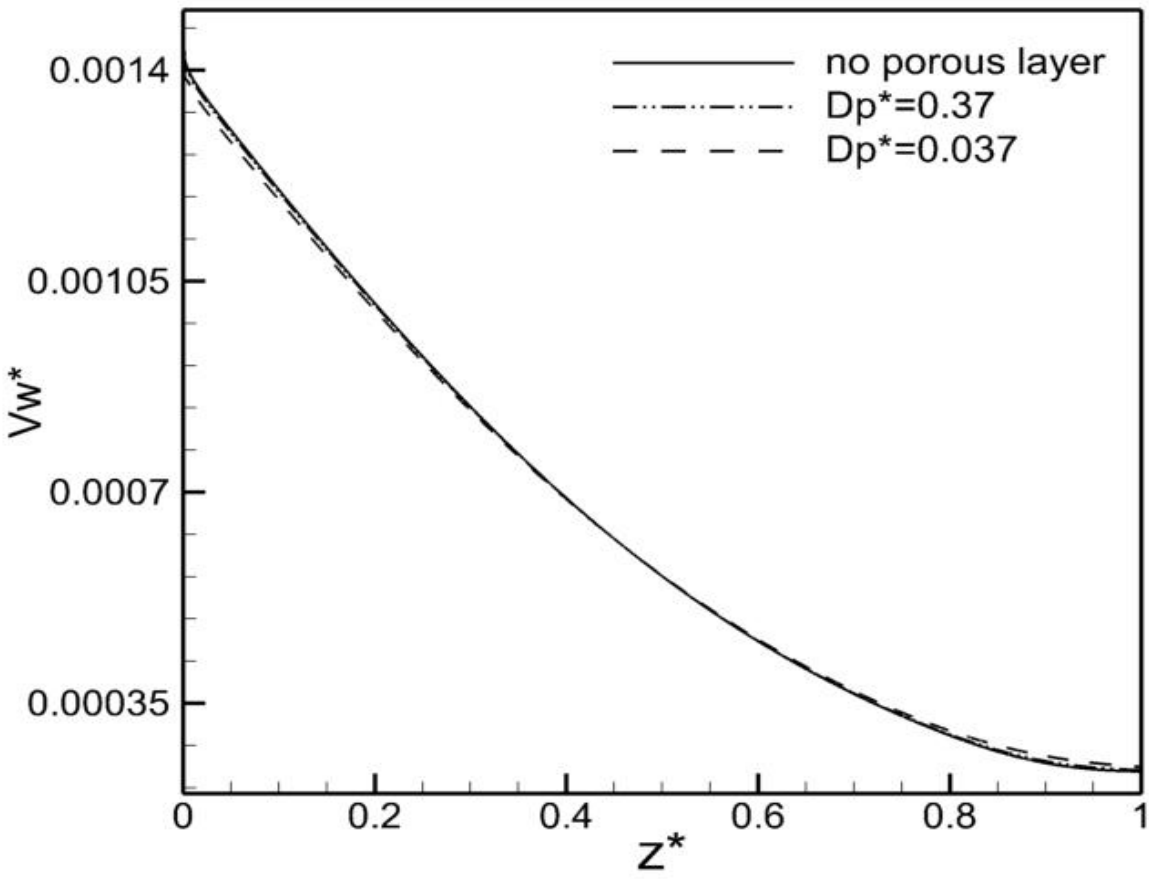

Figure 15: Normalized suction velocity at the membrane surface for different values of Dp* at Re = 30

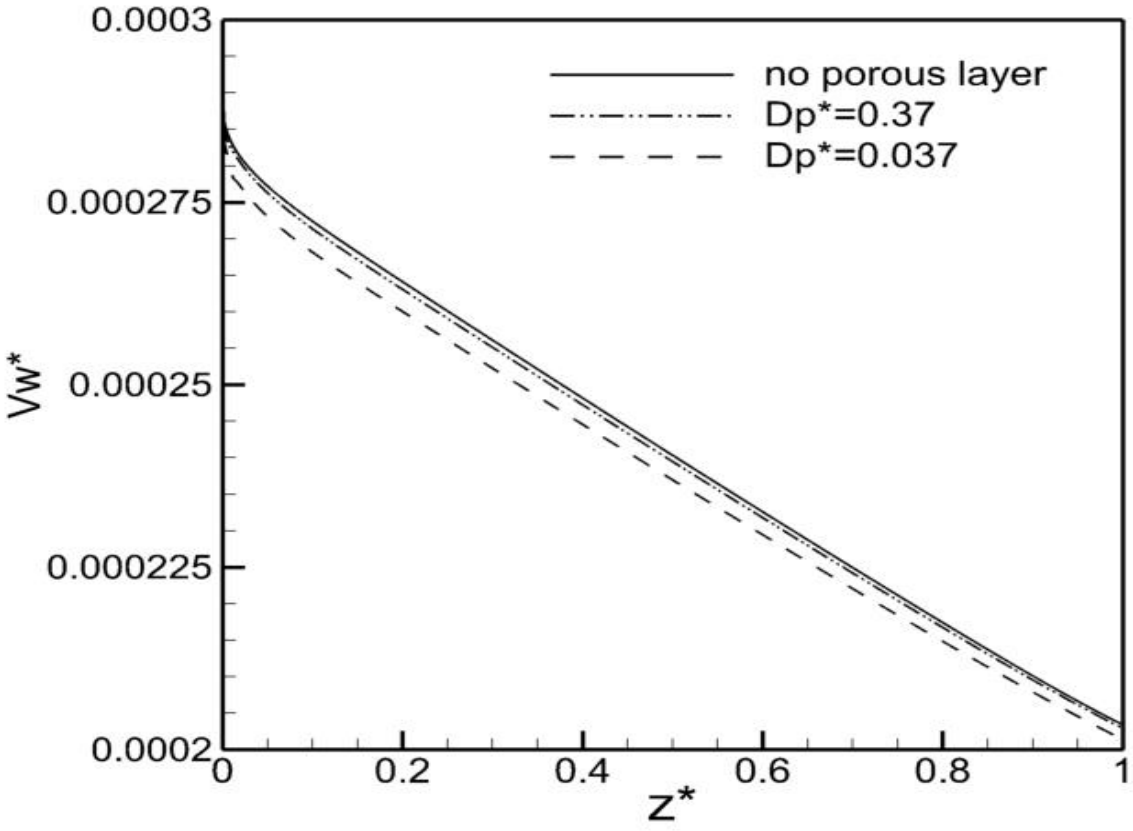

Figure 16: Normalized suction velocity at the membrane surface for different values of Dp* at Re = 150.

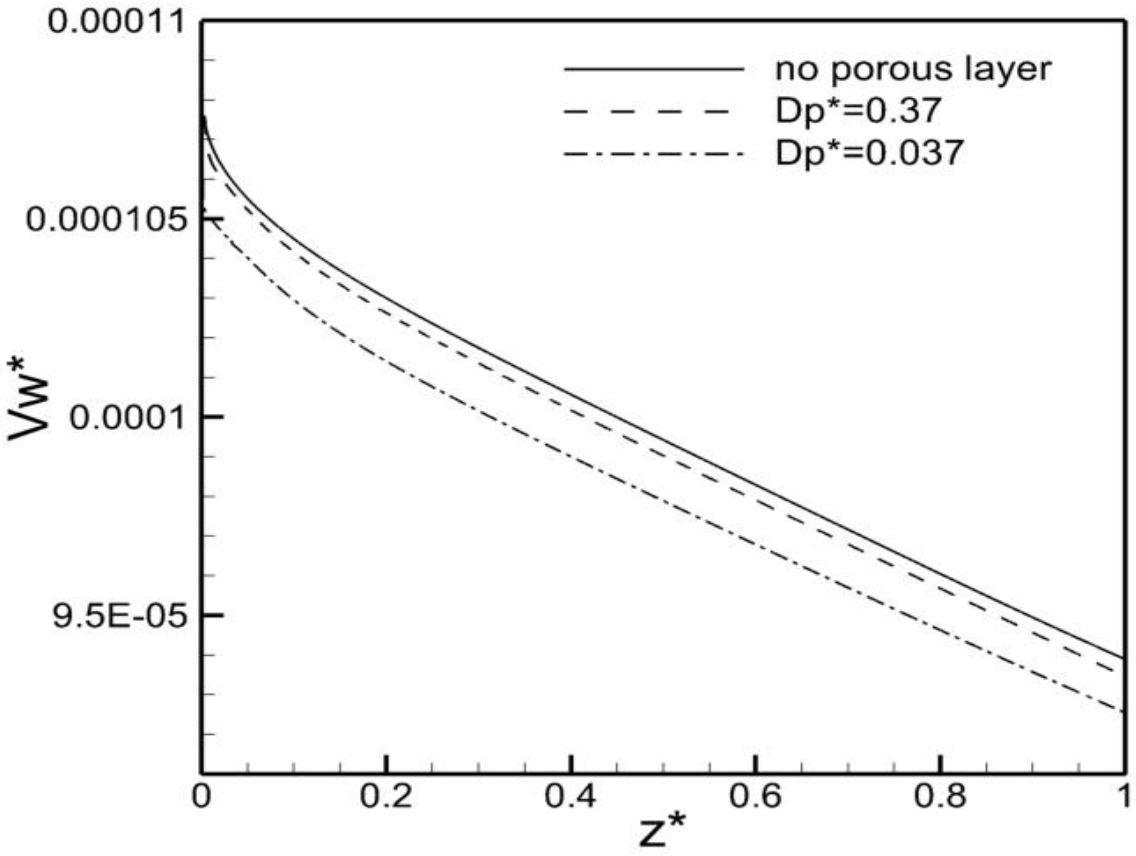

Figure 17: Normalized suction velocity at the membrane surface for different values of Dp* at Re = 400.

The concentration along the membrane surface is illustrated in Figures 18 to 20. At lower Re flows, the effect off the porous layer on the concentration of the permeated flux is not obvious as it is in the case of a higher Reynolds number, as seen in Figure 18. The increase in Re with the decrease of Dp* reflects on as an increase in CH_4 concentration at the membrane surface. This is because the flow escapes, due to increased resistance, to the open channel flow as Re increases. This fact was experimentally observed by G. Beavers et al [15].

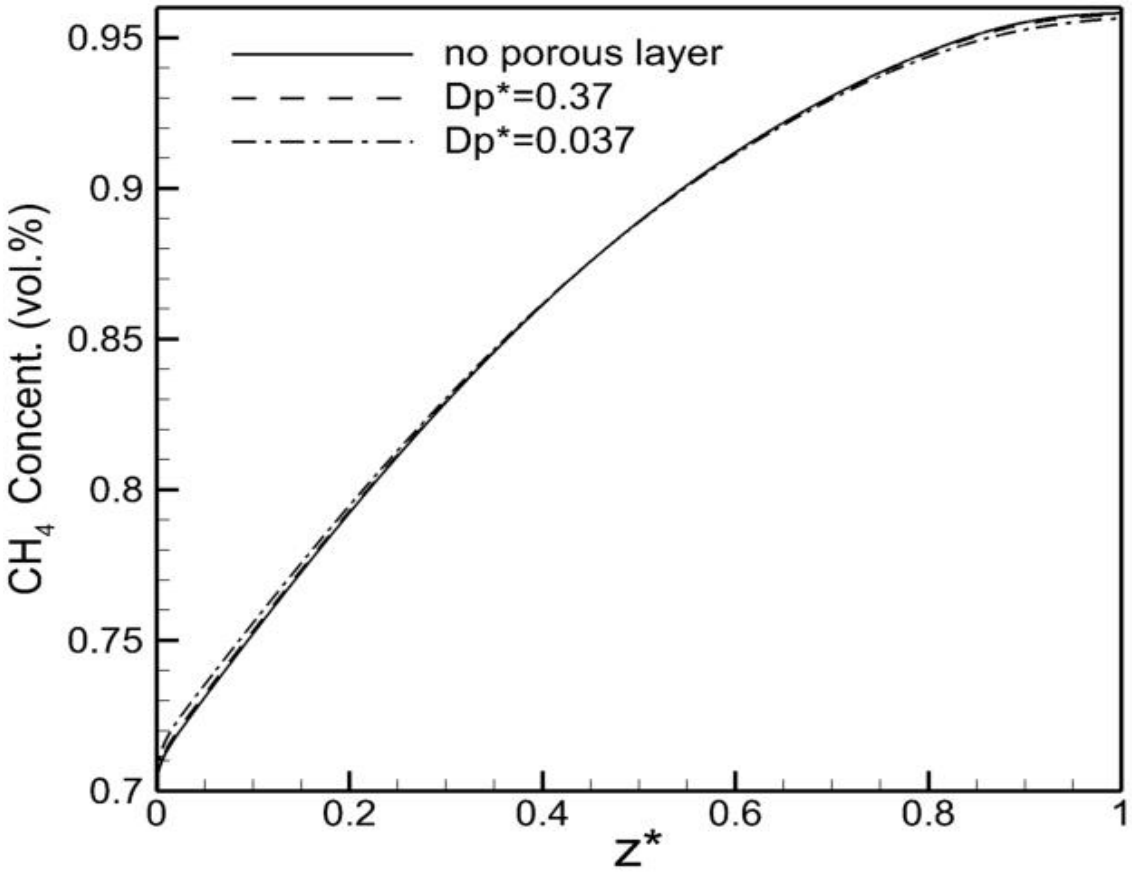

Figure 18: Concentration profiles at the membrane surface for different values of Dp* at Re = 30.

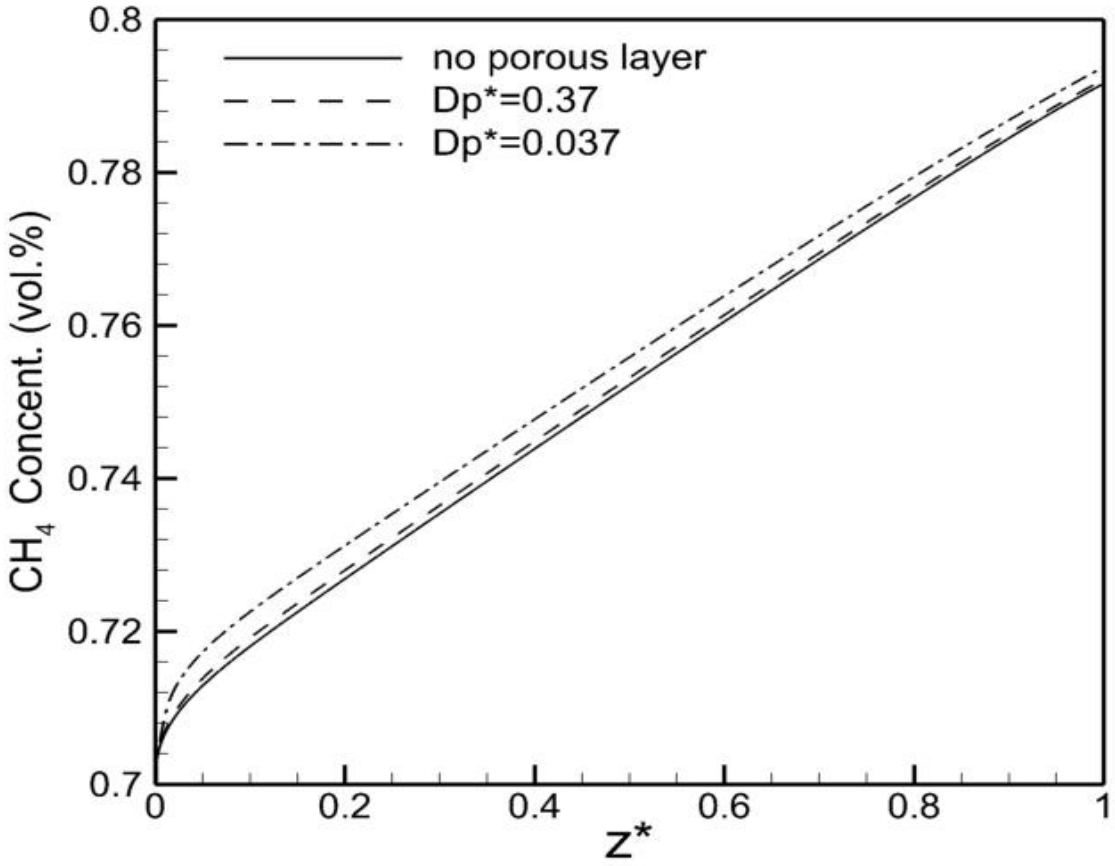

Figure 19: Concentration profiles at the membrane surface for different values of Dp* at Re = 150.

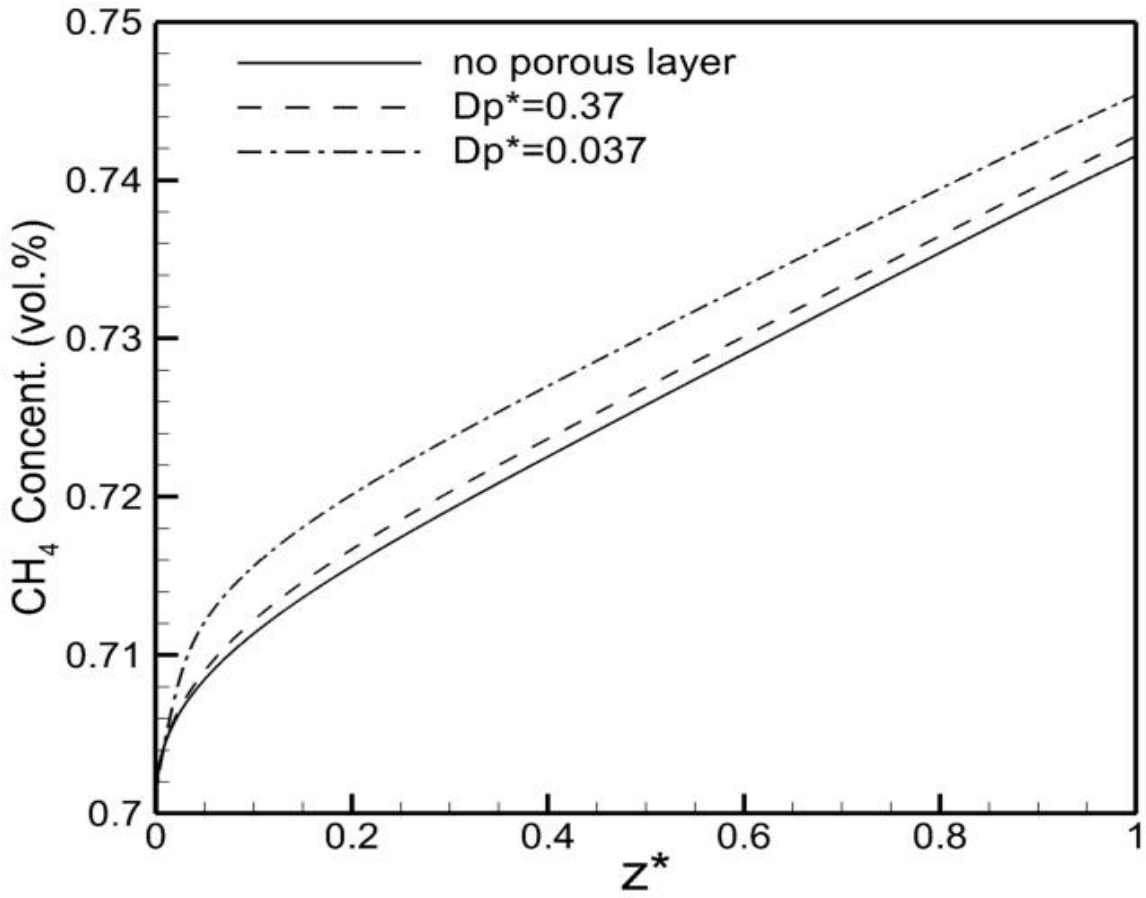

Figure 20: Concentration profiles at the membrane surface for different values of Dp* at Re = 400.

Figures 21 and 22 show CH_4 and CO_2 mass fluxes through the membrane as a percentage of their respective total mass at the inlet. The relative mass fluxes are calculated at different values of Re number and Dp*. Both Figures shows a decrease in the mass fluxes of CH_4 and CO_2 as Dp* decreases. This decreases in the total relative mass fluxes of CH_4 and CO_2 are more obvious at lower Re flows. However, CH_4 and CO_2 fluxes drop significantly as Re increases and asymptotes to zero due to the fact that

residence time of the mixture of CH_4 and CO_2 in the computation domain considered in the present study decreases as Re is increased.

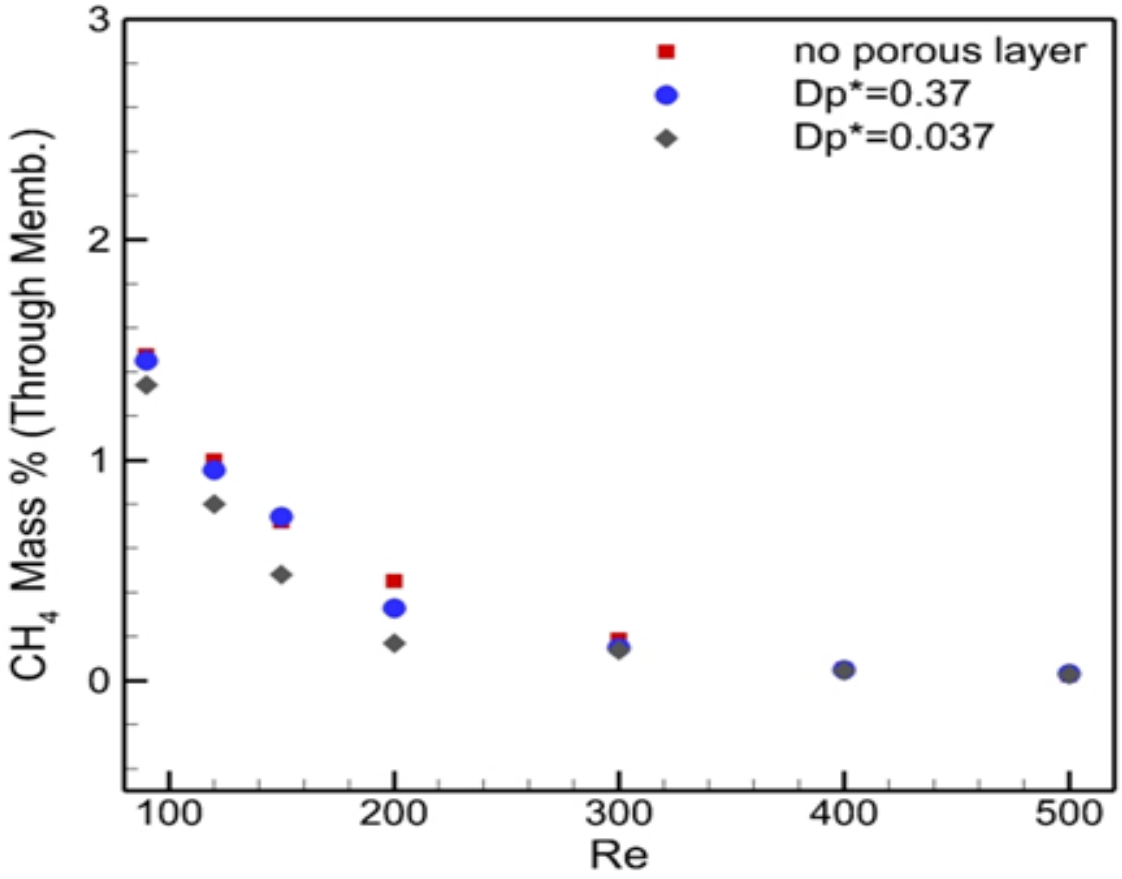

Figure 21: The relative mass flux of CH_4 passing through the membrane at Re = 400.

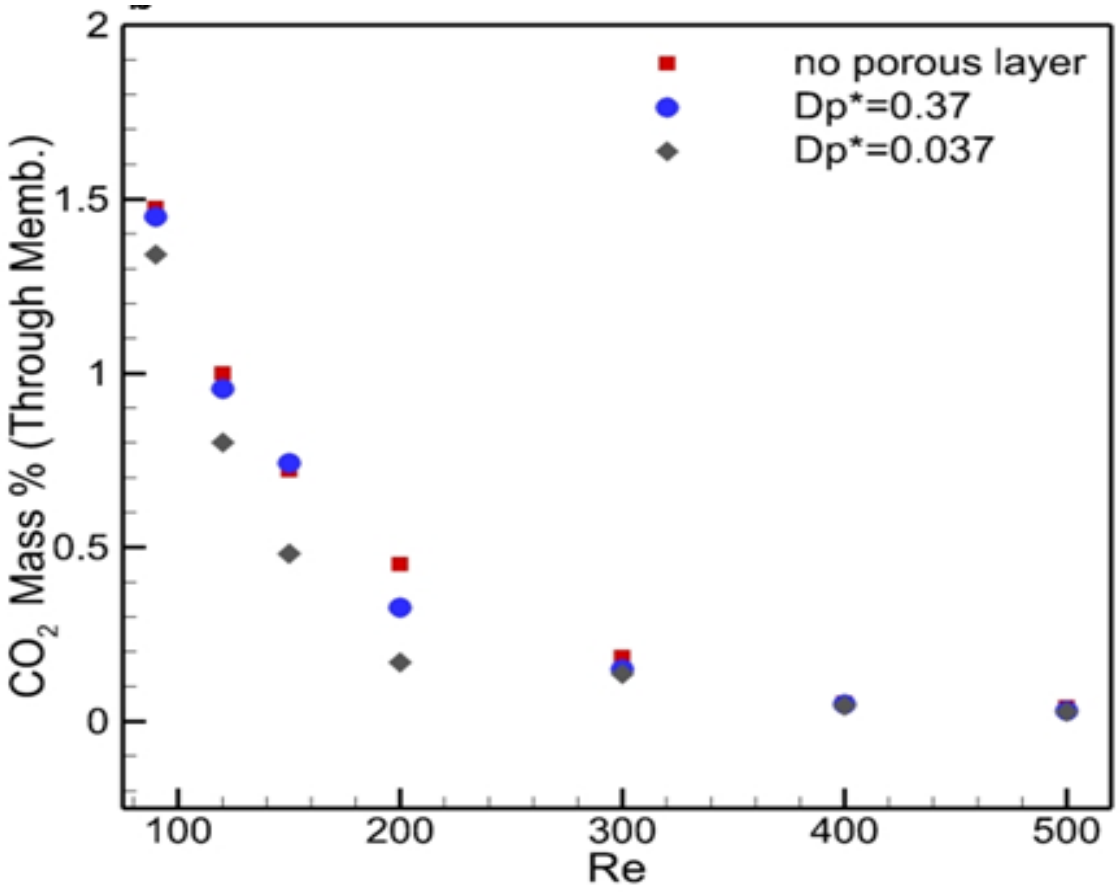

Figure 22: The relative mass flux of CO_2 passing through the membrane mass flux at Re = 400.

Sherwood number Sh is illustrated in Figure 23 for different values of Dp* at Re =400. Although the percentage of mass flux of species significantly decrease by the increase of Re, the presence of the porous layer appears to have a visible effect on Sh and thus on mass transfer as Dp* decreases.

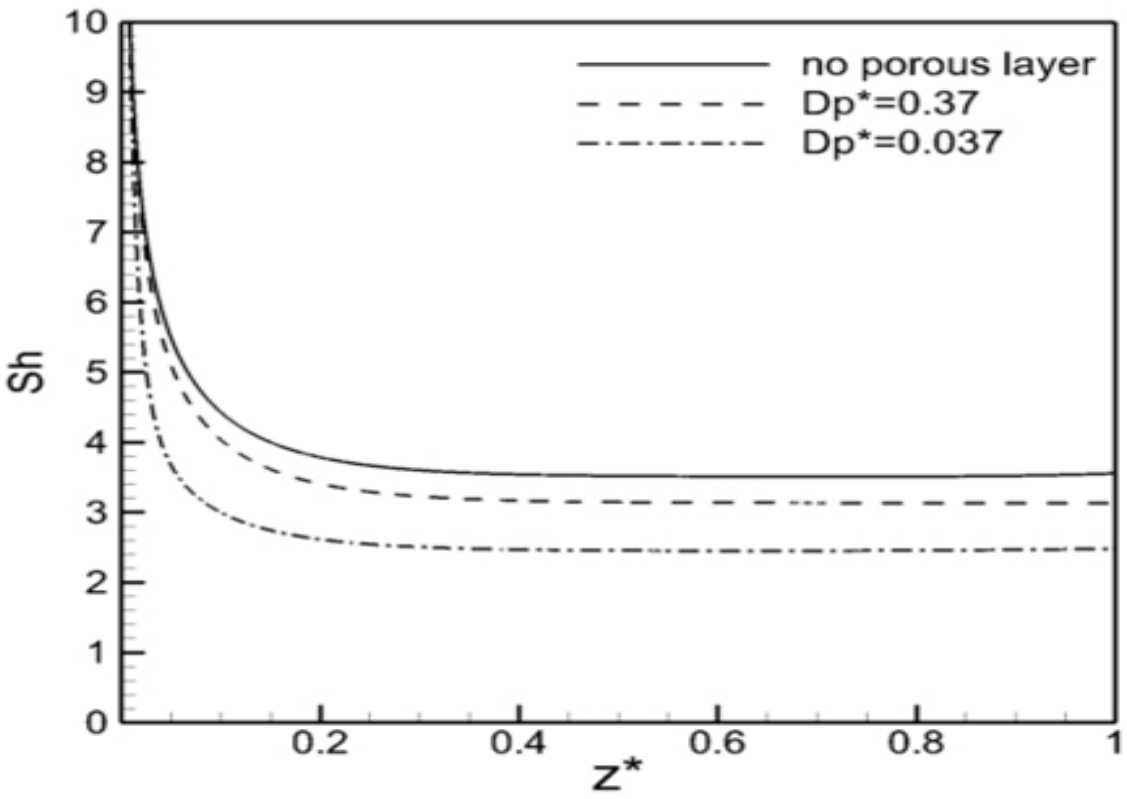

Figure 23: The local value of Sherwood number vs z/d calculated at Re = 400 for different values of Dp*.

5. Conclusion

The gas-gas separation using a membrane supported by a porous layer is studied using computational fluid dynamics simulations. The flow geometry is a circular cross-sectioned pipe. The separation of CO_2 in a CH_4 and CO_2 mixture is investigated for steady axisymmetric flows. The porous layer occupies 17% of the fiber diameter for the hollow fiber membrane module used in the present study. The effect of the porous layer on the membrane performance is determined for a wide range Reynolds numbers. The effect of the permeability and the thickness of the porous layer is also examined. A selective membrane bounds both the channel and the porous walls. Flow in the lumen side (channel and porous walls) is modeled using Navier-Stokes and Darcy's equations. Darcy's law is used to determine the flow and the pressure fields in the porous medium. For the permeability and the porosity of the porous medium considered here Darcy's law is proven to accurately represent the flow field. Mass flux of each species passing through the membrane is determined from the local pressure and the concentration.

The effect of the porous layer on the flow field in the open channel is very strong for the range of Re studied here. As the permeability of the porous medium is lowered or the thickness of the porous medium is increased the resistance to the flow in the porous layer is increased. Flow rate through the porous medium decreases while the flow rate through the open channel increases as the resistance of the porous layer is increased. The presence of the porous layer has a profound effect on the membrane performance. Mass flux of both CH_4 and CO_2 is lowered by the porous layer. The porous medium results in an increased pressure drop as the resistance of the porous medium is increased. Sherwood

number is significantly reduced as the resistance of the porous layer is increased. It is shown here that the porous layer should be an integral part of the hollow fiber membrane system modeling.

6. Bibliography

[1] B.D. Bhide, A. Voskericyan, S.A. Stern, Hybrid processes for the removal of acid gases from natural gas, Journal of Membrane Science, 140 (1998) 27-49.

[2] R.W. Baker, K. Lokhandwala, Natural Gas Processing with Membranes: An Overview, Industrial & Engineering Chemistry Research, 47 (2008) 2109-2121.

[3] S. Veríssimo, K.V. Peinemann, J. Bordado, New composite hollow fiber membrane for nanofiltration, Desalination, 184 (2005) 1-11.

[4] A. Broeckmann, J. Busch, T. Wintgens, W. Marquardt, Modeling of pore blocking and cake layer formation in membrane filtration for wastewater treatment, Desalination, 189 (2006) 97-109.

[5] P.K. Kundu, A. Chakma, X. Feng, Modelling of multicomponent gas separation with asymmetric hollow fibre membranes—methane enrichment from biogas, The Canadian Journal of Chemical Engineering, 91 (2013) 1092-1102.

[6] P.K. Kundu, A. Chakma, X. Feng, Simulation of binary gas separation with asymmetric hollow fibre membranes and case studies of air separation, The Canadian Journal of Chemical Engineering, 90 (2012) 1253-1268.

[7] M.J. Thundyil, W.J. Koros, Mathematical modeling of gas separation permeators — for radial crossflow, countercurrent, and cocurrent hollow fiber membrane modules, Journal of Membrane Science, 125 (1997) 275-291.

[8] C.Y. Pan, Gas separation by high-flux, asymmetric hollow-fiber membrane, AIChE Journal, 32 (1986) 2020-2027.

[9] T. Sugiyama, N. Miyahara, M. Tanaka, K. Munakata, I. Yamamoto, A simulation model for transient response of a gas separation module using a hollow fiber membrane, Fusion Engineering and Design, 86 (2011) 2743-2746.

[10] H.-Y. Zhang, R. Wang, D.T. Liang, J.H. Tay, Modeling and experimental study of CO2 absorption in a hollow fiber membrane contactor, Journal of Membrane Science, 279 (2006) 301-310.

[11] P. Keshavarz, J. Fathikalajahi, S. Ayatollahi, Mathematical modeling of the simultaneous absorption of carbon dioxide and hydrogen sulfide in a hollow fiber membrane contactor, Separation and Purification Technology, 63 (2008) 145-155.

[12] A.F. Portugal, F.D. Magalhães, A. Mendes, Carbon dioxide removal from anaesthetic gas circuits using hollow fiber membrane contactors with amino acid salt solutions, Journal of Membrane Science, 339 (2009) 275-286.

[13] S. Shirazian, A. Moghadassi, S. Moradi, Numerical simulation of mass transfer in gas–liquid hollow fiber membrane contactors for laminar flow conditions, Simulation Modelling Practice and Theory, 17 (2009) 708-718.

[14] B. Chen, Z. Gao, W. Jin, S. Zheng, Analytical mass transfer solution of longitudinal laminar flow of Happel's free surface model, International Journal of Heat and Mass Transfer, 54 (2011) 4000-4008.

[15] G.S.-S. Beavers, E. M.; Magnuson, R. A., Experiments on Coupled Parallel Flows in a Channel and a Bounding Porous Medium, J. Basic Eng., 92 (1970) 6.

[16] S.K. Karode, Laminar flow in channels with porous walls, revisited, Journal of Membrane Science, 191 (2001) 237-241.

[17] V. Nassehi, Modelling of combined Navier–Stokes and Darcy flows in crossflow membrane filtration, Chemical Engineering Science, 53 (1998) 1253-1265.

[18] R. Ghidossi, J.V. Daurelle, D. Veyret, P. Moulin, Simplified CFD approach of a hollow fiber ultrafiltration system, Chemical Engineering Journal, 123 (2006) 117-125.

[19] N.S. Hanspal, A.N. Waghode, V. Nassehi, R.J. Wakeman, Development of a predictive mathematical model for coupled stokes/Darcy flows in cross-flow membrane filtration, Chemical Engineering Journal, 149 (2009) 132-142.

[20] B. Marcos, C. Moresoli, J. Skorepova, B. Vaughan, CFD modeling of a transient hollow fiber ultrafiltration system for protein concentration, Journal of Membrane Science, 337 (2009) 136-144.

[21] D.A. Nield, A. Bejan, Convection in porous media, 3rd ed., springer, NY, 2006.

[22] O. Zikanov, Essential computational fluid dynamics, John Wiley & Sons, 2010.

[23] Incropera, Dewitt, Bergman, Lavine, Introduction to Heat Transfere, Wiley, 2007, pp. 489.

[24] E. Ucar, M. Mobedi, I. Pop, Effect of an Inserted Porous Layer Located at a Wall of a Parallel Plate Channel on Forced Convection Heat Transfer, Transp Porous Med, 98 (2013) 35-57.

7. Vita

Abdulmohsen Alsaiair was born on Nov. 5th,1983, in the city of Khamees Mushait, Saudi Arabia. He is the son of Omar Alsaiari and Latifah Sultan. Late 2001, Abdulmohsen graduated from Jareer High and decided to study mechanical engineering at King Abdulaziz University; started 2002. He graduated with a Bachelor of Science Degree in Mechanical Engineering in 2007 and right after joined the Saudi Aramco Company; Yanbu Refiner Department. He worked there as a maintenance and technical support engineer for a period of two years. In 2009, Abdulmohsen joined the Mechanical Engineering department at King Abdulaziz University where he worked as a research assistant; a positioned that granted him a scholarship to pursue a graduate level degree. He joined the Mechanical Engineering graduate program at Lehigh University in the summer of 2012. Abdulmohsen was awarded his Master of Science Degree in Mechanical Engineering from Lehigh University in May 2014.